Chapter 4

Characterization of Coplanar waveguide : Shunt circuit model

4.1 : Introduction

For complete understanding, characterization and optimization of a coplanar waveguide (CPW) phase shifter or similar transmission line device on a lossy semiconductor substrate, a good shunt circuit model is essential. In the model the lumped shunt circuit elements should be assessed to predict both the low and high frequency behavior. The shunt circuit model in conjunction with conductor loss calculations (i.e., the series circuit model), should provide a complete equivalent circuit picture of the device. In this chapter, using an accurate shunt circuit model, a detailed understanding of the CPW device is presented from a quasi-static perspective. A general description of the device including the basic quasi-static theory and the mode of its operation are discussed. Low frequency current-voltage (I-V) and capacitance-voltage (C-V) characteristics are also explained both from theoretical and experimental points of view. Frequency dependence of capacitance is also investigated under different bias conditions, and is compared with the measured results. High frequency behavior for the same model is also presented with experimental results, establishing the accuracy and the completeness of the model. The model identifies the main mechanism of rf propagation along a Schottky-contacted planar transmission line and gives a physical explanation for the change of propagation characteristics both with voltage and optical power over a wide range of operating frequencies. Comparisons are also made for an MIS (Metal-Insulator-Semiconductor) CPW structure on a Si-SiO_2 substrate, which comprises an ideal slow-wave configuration, both with the measured and other existing model results. At the end of this chapter, some model-predicted optimization issues are discussed, where the effect of background conductivity, bias voltage, and operating frequency on the change of attenuation constant and

effective index of refraction, n_{eff} ($=\beta/\beta_o$, also known as slow wave factor), are shown.

4.2. : Basic quasi-static theory

The coplanar waveguide structure, used as a voltage or optically controlled device, usually consists of three layers as shown in Fig. 4.1. The top-most layer (labeled region 1) is a lossless region, such as an insulator layer or a depletion region formed due to metal-semiconductor Schottky contact. Region 2, the lossy layer, usually consists of epitaxially GaAs. Region 3 is again a lossless layer, such as semi-insulating GaAs or quartz. On the top of this multi-layered substrate, three parallel metal electrodes are deposited, as shown in Fig. 4.1. The wide outer conductors are ground planes and the center conductor is the signal line.

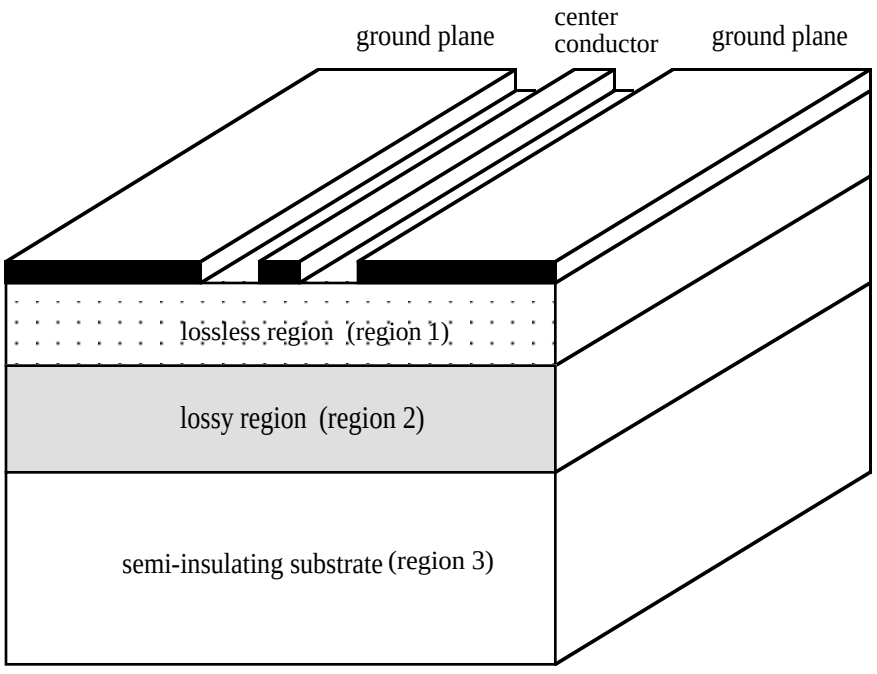

Figure 4.1 : Schematic diagram of a multi-layered coplanar waveguide (CPW).

For the CPW geometry, the width of the center conductor and the gap between the center conductor and ground planes are the main features which determine the nature of wave propagation in the CPW. For a CPW in free space, if the center conductor and gap widths are much smaller than a wavelength, only a TEM wave should be able to propagate on the line. With such conductor geometries it is expected that a quasi-TEM wave will propagate on a substrate-supported CPW. In addition, the field penetration into the substrate is roughly comparable to the width of the gap. Therefore, if the lossy layer in the substrate is near the surface (compared to gap size), it can have a significant effect on device performance.

It is possible to understand device operation using quasi-static approximations if the center conductor width, gap width, and the layer thicknesses are all much smaller than a wavelength in size. The basic parameters which may affect

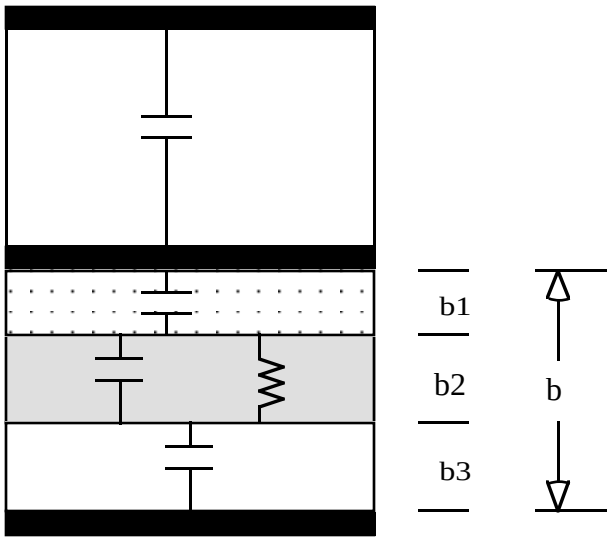

Figure 4.2 : Simplified parallel plate model for a co-planar waveguide, where the bottom region consists of semiconducting layers and top region represents the air-side of the CPW.

the propagation constant can be found by considering a simple parallel plate model for a transmission line, as shown in Fig. 4.2. Figure 4.2 shows the simplified shunt circuit where the top two parallel plates comprise the air region and bottom two plates take care of the multi-layered semi-conducting materials. In the bottom parallel plate model, three distinct regions are shown, where the first (b1) and third layers (b3) are both lossless, whereas the middle layer (b2) is the lossy region which has finite conductance in addition to capacitance. This simplified picture leads us to calculate the shunt admittance, Y, and the series impedance, Z separately (as shown in Fig. 4.3), considering static electric and static magnetic fields, respectively.

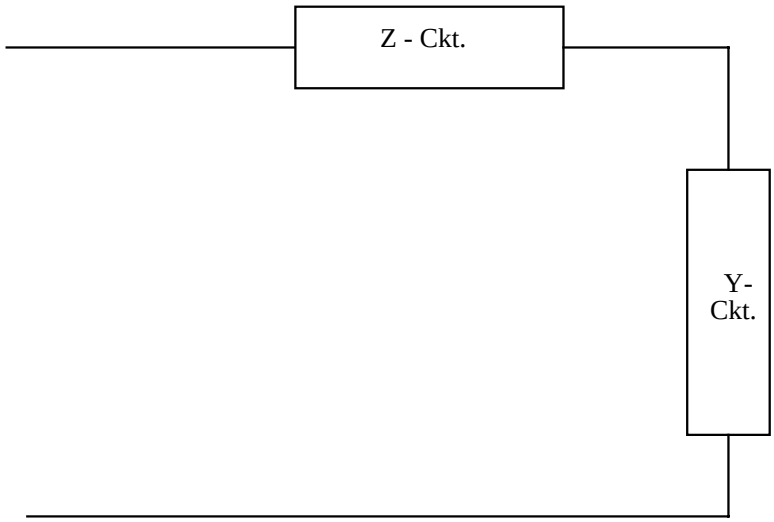

Figure 4.3 : Simplified equivalent circuit, where series element, Z, and shunt element, Y, can be calculated separately considering static magnetic field and static electric field, respectively.

For the analysis of shunt admittance as a function of frequency, the dielectric relaxation frequency for the lossy layer is a very important parameter. The dielectric relaxation frequency for this lossy layer is

$$f_{\mathrm{dr}} = \frac{\sigma}{2\pi\varepsilon_O\varepsilon_r} \tag{4.2.1}$$

where ε_r and σ are the relative dielectric constant and the conductivity of the lossy layer. If the frequency of the applied voltage is much lower than the dielectric relaxation frequency f_{dr}, the free charges in the lossy layer can respond to the applied voltage. As a result the lossy layer behaves as a "conductor-like" material and effectively forms a short between the two lossless layers. Hence the admittance per unit length, Y of the structure becomes

$$Y = j\omega C_L = j\omega\left(\frac{1}{C_1}+\frac{1}{C_3}\right)^{-1} = j\omega\varepsilon_o\varepsilon_r\left(\frac{a}{b_1+b_3}\right) = j\omega\varepsilon_o\varepsilon_r\left(\frac{a}{b-b_2}\right) \tag{4.2.2}$$

where $b=b_1+b_2+b_3$, and a is the total width of the device as shown in Fig. 4.2. When the frequency of the applied field becomes much higher than the dielectric relaxation frequency, the lossy layer free charges can no longer follow the field. As a result, the lossy layer acts as a dielectric. In this case, the admittance is determined by

$$Y = j\omega C_H = j\omega\left(\frac{1}{C_1}+\frac{1}{C_2}+\frac{1}{C_3}\right)^{-1} = j\omega\varepsilon_o\varepsilon_r\left(\frac{a}{b}\right). \tag{4.2.3}$$

From this analysis it is clear that in the limiting cases the "low" frequency capacitance (C_L) is higher than the "high" frequency capacitance (C_H).

Evaluation of series impedance has already been discussed in detail in chapter 3. From simple magnetostatic perspective, it can be approximated that series impedance, Z comprises of only the external inductance of the parallel plates for a lossless case, as

$$Z = j\omega L = j\omega\mu_o \frac{b}{a}. \tag{4.2.4}$$

Propagation velocity and propagation constant can now be calculated using

$$\gamma = j\omega\sqrt{LC} \tag{4.2.5}$$

$$v = \frac{1}{\sqrt{LC}}. \tag{4.2.6}$$

Therefore, for f_{op} (operating frequency) << f_{dr}, the velocity v, and propagation constant γ, becomes

$$v = \frac{1}{\sqrt{LC}} = \frac{1}{\sqrt{\left(\mu_o \frac{b}{a}\right)\left(\varepsilon_o\varepsilon_r \frac{a}{b-b_2}\right)}} = \frac{v_{vac}}{\sqrt{\varepsilon_r}}\sqrt{1-\Delta} \tag{4.2.7}$$

$$\gamma = j\omega\sqrt{\mu_o\varepsilon_o\varepsilon_r}(1-\Delta)^{-1/2} \tag{4.2.8}$$

where Δ is the filling fraction of the lossy layer, i.e., b_2/b, and v_{vac} is the speed of light in free space. Again for $f_{op} >> f_{dr}$ the velocity, v, and the propagation constant γ, becomes

$$v = \frac{1}{\sqrt{LC}} = \frac{1}{\sqrt{\left(\mu_o \frac{b}{a}\right)\left(\varepsilon_o\varepsilon_r \frac{a}{b}\right)}} = \frac{v_{vac}}{\sqrt{\varepsilon_r}}, \tag{4.2.9}$$

$$\gamma = j\omega\sqrt{\mu_o\varepsilon_o\varepsilon_r}. \tag{4.2.10}$$

It is evident from here that at "low" frequencies, higher capacitance leads to lower propagation velocity than that at "high" frequencies. This shows the origin of the "slow wave" at lower frequencies.

4.3. Earlier explanations for changing device characteristics

For "low" frequency operation, the propagation constant, β (and thus the phase), can be varied by changing the thickness of the lossy layer. This can be achieved by changing the bias voltage if the depletion region formed due to metal-semiconductor Schottky contact is used as the first insulating layer. Instead of changing the bias voltage, injection of photons with energy higher than the bandgap of GaAs can also change the width of the depletion region due to generation of electron-hole pairs. With high level injection, it may also change the conductivity of the lossy layer, which would in turn change the dielectric relaxation frequency. Changing the depletion region thicknesses with bias voltage or optical power basically changes the capacitance, as described in the earlier section, and hence changes the phase constant. This change is shown conceptually in Fig. 4.4(a). In contrast, with high-level injection, the change of phase is achieved by changing the dielectric relaxation frequency limit, as shown in Fig. 4.4(b).

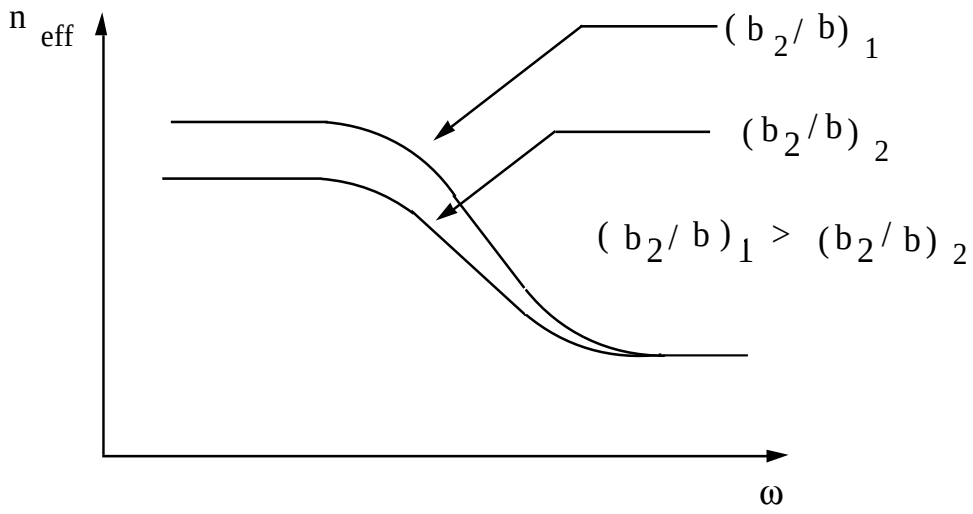

Figure 4.4(a) : Dispersion curve for Schottky control, where change in thicknesses of lossy and lossless layers is achieved through application of a bias voltage.

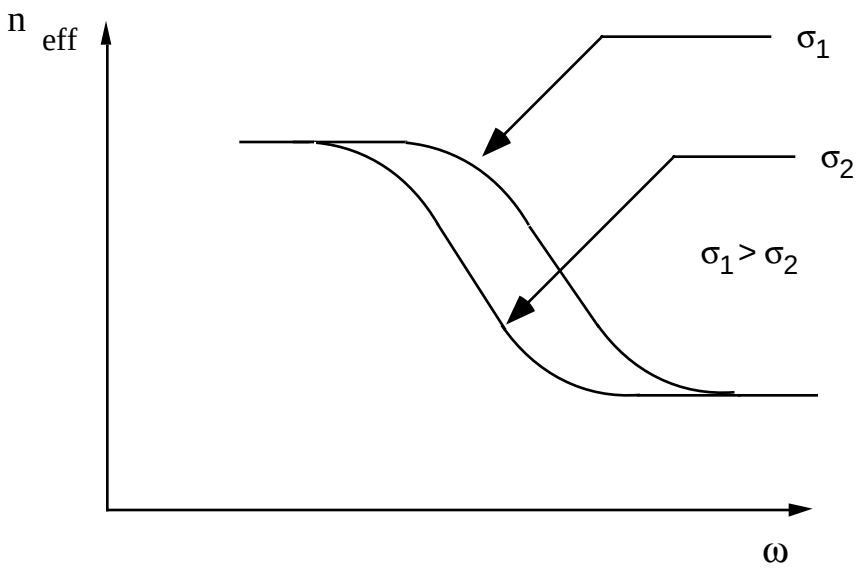

Figure 4.4(b) : Dispersion curve for optical control only, when the dielectric relaxation frequency limit is changed with high level injection.

The explanation presented above has limited success in predicting exact voltage and frequency dependence of the propagation constant of a Schottky-contacted CPW, especially with the samples used in this study. To explain its limitations, first of all, it is necessary to describe the material, geometry, and frequency range that has been used. The frequency range for the measurements is 45 MHz to 40 GHz. The material of interest is GaAs, which has a relative dielectric constant of 13. For this material the dielectric wavelength at different frequencies are

at 40 MHz	λ_d = 210 cm
at 1 GHz	λ_d = 8.3 cm
at 40 GHz	λ_d = 0.21 cm
at 100 GHz	λ_d = 830 μm

In our CPWs the center conductor width is 10 μm and the gap is 7 μm with lossy layer thickness in the range of 1 to 10 μm. Therefore even at the highest frequency of the measurement (40 GHz) the signal line and the gap widths are much smaller than the wavelength in the semiconductor layer. The dielectric relaxation frequency limits for different conductivities of GaAs are as follows

p-type:	$N_A = 10^{15}/cm^3$,	$\rho = 20\ \Omega$-cm,	$f_{dr} = 7$ GHz
n-type:	$N_D = 10^{15}/cm^3$,	$\rho = 1.5\ \Omega$-cm,	$f_{dr} = 90$ GHz
n-type:	$N_D = 10^{16}/cm^3$,	$\rho = 0.15\ \Omega$-cm,	$f_{dr} = 900$ GHz
n-type:	$N_D = 10^{17}/cm^3$,	$\rho = 0.015\ \Omega$-cm,	$f_{dr} = 9$ THz

Therefore, for n-type GaAs samples even at the lowest conductivities (the MBE material used here was typically doped n-type in the range of $10^{15}/cm^3$) the dielectric relaxation frequency limits (~90 GHz) are well above the highest frequency of measurement (40 GHz). This directly shows that the change of phase using optical power only can not occur, since illumination can only increase the dielectric relaxation frequency. In addition, by moving the depletion layer edge only through bias voltage or optical illumination, the calculated change in low frequency capacitance from the simple model does not match with that of experimental results. Also, change in capacitance by change in area [Capasso et al. 1982; Tsai et al. 1991] or width [Cheung et al. 1990] is not sufficient to explain the amount of change in device propagation characteristics. All these discrepancies are avoided in the proposed R_{epi}-C shunt model, where the change in device characteristics are attributed mostly to the change in the lossy layer sheet resistance, which is in series with the depletion region capacitance.

4.4 : Simple circuit models

To further understand the operating mechanism of a Schottky-contacted co-planar waveguide phase shifter, three simple models are introduced. In the first

model (model 1) an L - C circuit is considered, as shown if Fig. 4.5(a). The inductance per unit length, L, is taken as the quasi-static inductance of a CPW, evaluated using a standard conformal mapping technique [Wen 1969; Wentworth et al. 1989]. Capacitance in the shunt circuit is taken as a voltage dependent depletion capacitance, calculated using a one-dimensional depletion approximation. This model represents an ideal slow wave structure if C_{dep} is replaced by $C_{dielectric}$. In the slow wave model effective capacitance increases as frequency is decreased (and hence phase increases and effective index of refraction, n_{eff}, increases) below the dielectric relaxation frequency limit due to a strong interfacial polarization [Hasegawa et al. 1971], known as "Maxwell-Wagner Effect" [Hippel 1941]. In the case of a Schottky-contacted CPW structure with moderate to low sheet resistance of the lossy layer, the true low frequency capacitance has to be C_{dep}, because the undepleted lossy layer acts as a conducting plate. As shown in Fig. 4.6(a) and (b), n_{eff} calculated using this model is a flat line with respect to frequency at one particular bias voltage (at zero bias in Fig. 4.6(a) and at 2 volts bias in Fig. 4.6(b). The carrier concentration in the epi-layer is assumed to be $5x10^{15}$ /cm^3). This n_{eff} value matches neither the low frequency nor high frequency behavior of the experimental index of refraction. For model 1, at low frequency the shunt capacitance (C) is correct but the series inductance (L) is not: there is actually dc loss involved with the series circuit, which change the low frequency characteristics. At high frequency, L dominates over the series R, but then C_{dep} is not the correct C; rather the quasi-static capacitance, C_{CPW} needs to be considered. Two more simple models will verify this explanation. The second model (model 2) is comprised of an accurately evaluated Z circuit combined with C_{dep} (as shown in Fig. 4.5(b)) and the third one (model 3) uses the same Z and the quasi-static capacitance of the CPW structure (C_{CPW}) (as shown in Fig. 4.5(c)). The Z circuit components (Z_{CPW}) are calculated using a conformal mapping technique, which has shown excellent agreement with experimental results [Islam et al. 1993] . Model 2 has both frequency and voltage dependence, where the low frequency characteristics match that of the experimental measurements, because in the low frequency limit, the effective capacitance is only C_{dep} and the Z circuit is also valid

at all frequencies. The high frequency n_{eff} is higher than that of the experiment and approaches the L - C model value, because in the limit, where L dominates over R in the series circuit, the Z_{CPW} - C_{dep} model eventually becomes an L - C model. At low frequencies, n_{eff} is increased as frequency is decreased because of an R - C effect. Therefore, the experimental n_{eff} increases with decreasing frequency not because C is increased due to slow wave effect, but because of R-C type structure of the device. The third model with Z_{CPW} and C_{CPW} gets the correct high frequency n_{eff} value, because in the high frequency limit, C_{CPW} dominates over C_{dep}, but the low frequency n_{eff} is lower than that of the experiment since the low frequency dominant term in the shunt circuit, C_{dep}, is missing in this model. The shape in n_{eff} at lower frequencies is the same as that of experiment, which also verifies the fact that the increase in n_{eff} at lower frequencies is due to the R - C effect.

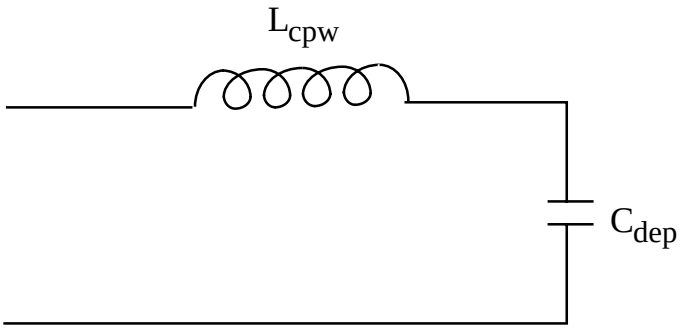

Figure 4.5(a) : Simple model with L_{CPW} and C_{dep} as the series and shunt circuits, respectively (model 1).

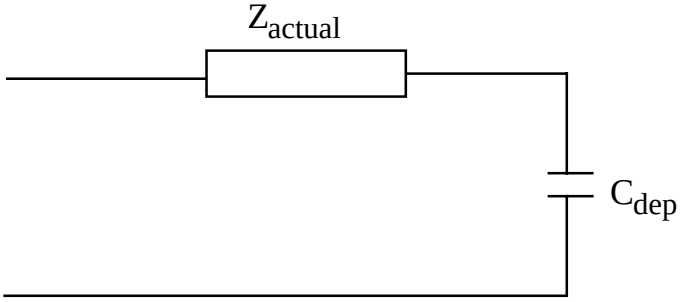

Figure 4.5(b) : Simple model with Z_{map} and C_{dep} as the series and shunt circuits, respectively (model 2).

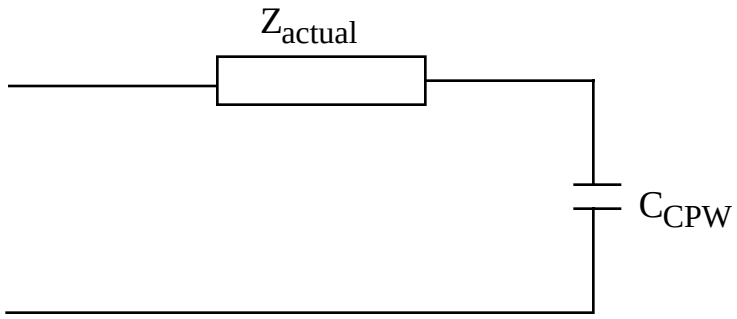

Figure 4.5(c) : Simple model with Z_{map} and C_{CPW} as the series and shunt circuits, respectively (model 3).

The explanations presented with these simple models suggest that a "good" model should incorporate C_{dep} at low frequency, C_{CPW} at high frequency, and the proper Z circuit at all frequencies. This can only be achieved by considering a series resistance underneath the depleted region capacitances (C_{dep}), which has negligible effect at lower frequencies, but prevents C_{dep} from contributing at higher frequencies. This describes the background for a R_{epi}-C model for a Schottky-contacted voltage controlled CPW model, which is discussed in detail in the next section. For comparison, in figures 4.6(a) and (b), n_{eff} values are also shown based on the complete equivalent circuit, as discussed in the next section, which is in good agreement with the measured values.

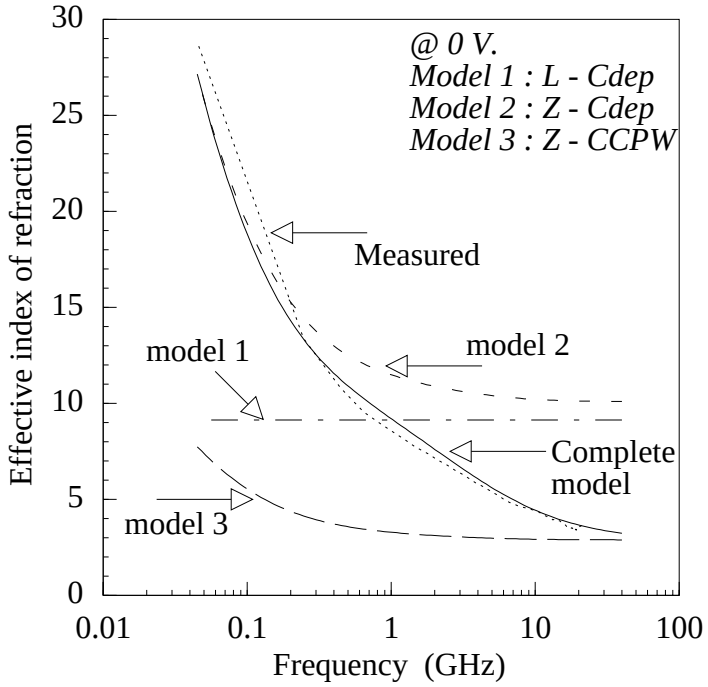

Figure 4.6(a) : Measured and modeled results for effective index of refraction (n_{eff}) for three simple models and for the complete model at a bias voltage of 0 V.

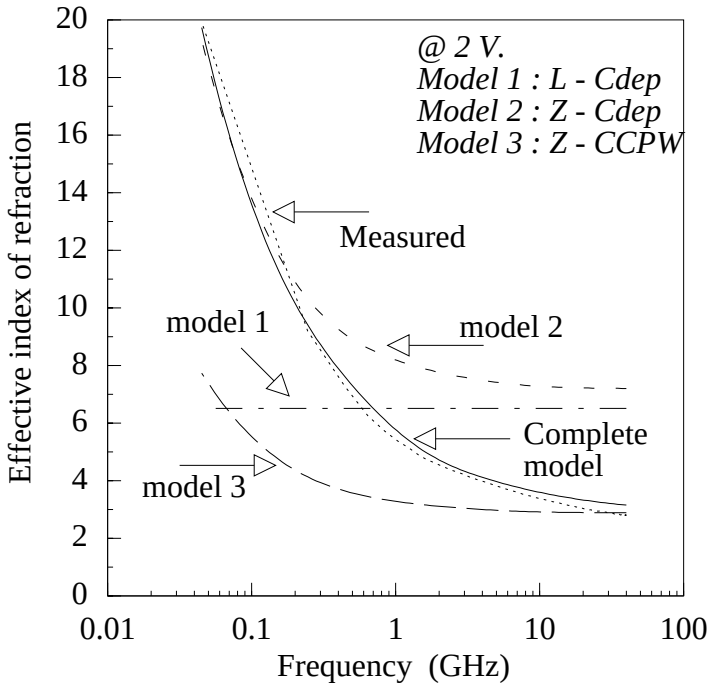

Figure 4.6(b) : Measured and modeled results for effective index of refraction (n_{eff}) for three simple models and for the complete model when the center conductor is biased at 2 V with respect to the ground planes.

4.5 : Proposed R_{epi}-C shunt circuit model

A Schottky-contacted coplanar waveguide phase shifter is assumed to consist of a lightly doped epitaxial layer on the top of a high resistivity substrate. The cross-sectional drawing is shown in Fig. 4.7(a) & 4.7(b), where Fig. 4.7(b) includes all the circuit parameters associated with the structure. The proposed R_{epi} - C shunt circuit model of this structure identifies the primary mechanism of propagation constant control, and its dependence on doping concentration, layer thickness, and applied voltage. In the shunt admittance per unit length, Y_{tot} , for the transmission line, the depletion regions under the CPW electrodes contribute a distributed capacitance, while the undepleted doped layers contribute a distributed resistance. Figure 4.8 shows the equivalent circuit that represents all the contributions to Y_{tot}. The distributed resistance of the undepleted regions forms a series R - C circuit [Wiley et al. 1975; Wiley 1978] with the distributed capacitance of the depleted layer. This series R - C circuit can be analyzed by transmission line theory, where resistances and capacitances per unit length can be defined as

$$\text{R / unit length} = \text{R}_\text{s} = \frac{1}{\sigma\left(\text{t}^{\text{epi}} - \text{h}\right)} \tag{4.5.1}$$

$$\text{C / unit length} = \frac{\varepsilon_\text{o}\varepsilon_\text{r}}{\text{h}} \tag{4.5.2}$$

where t^{epi} and h are the total epi layer and depleted layer thicknesses, respectively. σ and ε_r are the conductivity and relative dielectric constant of the semiconducting layer, respectively. R / unit length is defined as the sheet resistance, R_S . Because of symmetry, the CPW geometry can be divided into two as if having a magnetic wall at the mid-point of the center conductor. Both for center conductor and ground planes, the transmission line analyses can be carried on considering open-circuited RC transmission lines. In addition, a residual sheet resistance due to the high resistivity substrate, R_s^{back}, is assumed and added in parallel to the normal

sheet resistance of the epi layer. The sheet resistances of the various regions are calculated as

$$R_S^{gp} = \left(\sigma\left(t^{epi} - h^{gp}\right) + \frac{1}{R_S^{back}} \right)^{-1} \tag{4.5.3}$$

$$R_S^{cntr} = \left(\sigma\left(t^{epi} - h^{cntr}\right) + \frac{1}{R_S^{back}} \right)^{-1} \tag{4.5.4}$$

$$R_S^{gap} = \left(\sigma\left(t^{epi}\right) + \frac{1}{R_S^{back}} \right)^{-1} \tag{4.5.5}$$

where superscripts *gp*, *gap*, *cntr* and *back* stand for ground plane, gap, center conductor and background substrate regions, respectively. The normal CPW capacitance per unit length consists of an air side contribution (C_{air}) and a substrate side contribution (C_{sub}); these are easily found using standard conformal mapping techniques [Wen 1969; Wentworth et al. 1989]. The contributions from the depleted regions' capacitances per unit length are calculated as

$$C^{cntr} = \frac{\varepsilon}{h^{cntr}} \tag{4.5.6}$$

$$C^{gp} = \frac{\varepsilon}{h^{gp}} \tag{4.5.7}$$

where, *gp* and *cntr* stand for ground plane and center conductor, respectively. The impedances looking into the ground plane, *Zgp* and looking into the center conductor, *Zcntr*, as shown in Fig. 4.9, can be calculated using the per unit values of resistances and capacitances as defined in eqns. (4.5.3) - (4.5.7). The algebraic formulations for evaluating these impedances are given in Appendix A. These impedances, *Zgp* and *Zcntr* appear in equivalent circuit model (Fig. 4.8) and are given by

$$\mathbf{Z}^{gp} = \frac{\sqrt{\frac{R_S^{gp}}{j\,\omega\,C^{gp}}}}{\mathbf{tanh}\left(\gamma^{gp}\,w^{gp}\right)} \tag{4.5.8}$$

$$\mathbf{Z}^{cntr} = \frac{\sqrt{\frac{R_S^{cntr}}{j\,\omega\,C^{cntr}}}}{\mathbf{tanh}\left(\gamma^{cntr}\,a\right)} \tag{4.5.9}$$

where ω is the angular frequency, and γ^{gp} , γ^{cntr} are defined as follows

$$\gamma^{gp} = \sqrt{j\,\omega\,C^{gp}\,R_S^{gp}} \tag{4.5.10}$$

$$\gamma^{cntr} = \sqrt{j\,\omega\,C^{cntr}\,R_S^{cntr}}\,. \tag{4.5.11}$$

From *Zgp* and *Zcntr*, it is clear that if $\omega C R_S$ is small enough (i.e., if the frequency is low, or the undepleted epi layer is thick and has high enough conductivity), Z is just the parallel plate capacitance across the depletion region. However, if $\omega C R_S$ becomes large (e.g., when the depletion width approaches the thickness of the epi layer) the series resistance prevents the capacitance from contributing fully. Referring to Fig. 4.8, the total shunt admittance per unit length, Y_{tot} , for a Schottky-contacted CPW is

$$Y_{tot} = 2\left(j\omega C_{cpw}^{tot} + \frac{1}{Z^{cntr} + R^{gap} + Z^{gp}} \right) \tag{4.5.12}$$

where R^{gap} is the total gap region resistance, $R^{gap} = R_S^{gap}\left(b-a\right)$. The factor of two is from both sides, by symmetry. It is to be noted that when h^{gp} or h^{cntr} is very close to t^{epi}, i.e., the epi layer is almost fully depleted under the ground planes or center conductor, R_S becomes very high. Under such a condition, a very small variation in depletion region edge can cause a large change in R_S, and therefore, in propagation constant. This is what happens when the Schottky-contacted CPW is used as an optically controlled phase shifter, because even a very small amount of

optical power causes large change in R_s at or near the fully depleted bias voltage. Hence the optically-controlled device basically operates as a R_S controlled device, rather than as a capacitance controlled device.

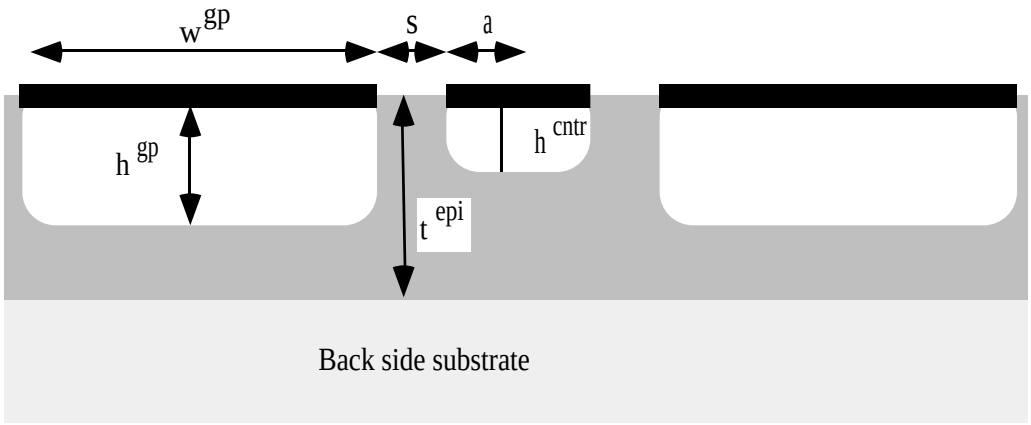

Figure 4.7(a) : Cross-sectional schematic of Schottky-contacted CPW on a doped semiconductor substrate.

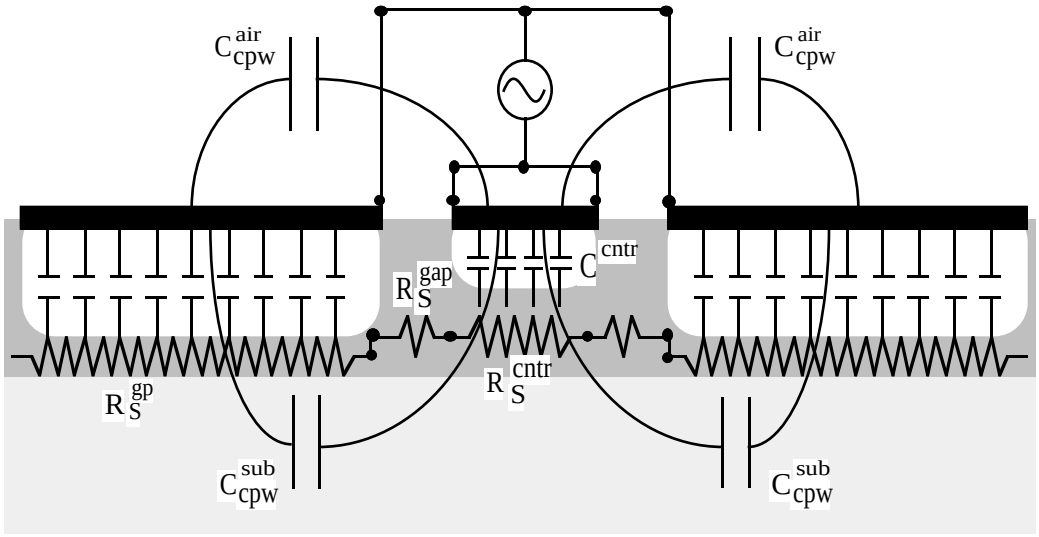

Figure 4.7(b) : Different circuit elements of the proposed R-C shunt model with the CPW schematic.

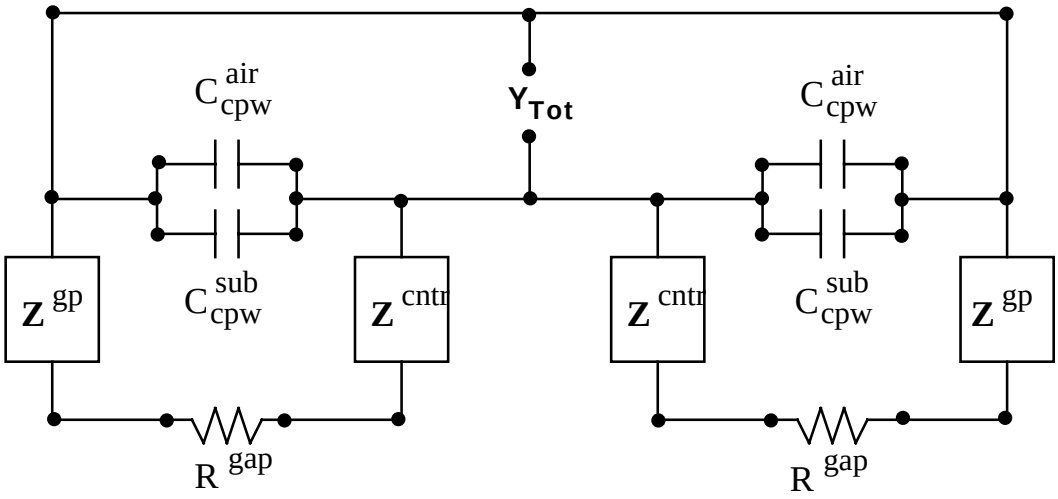

Figure 4.8 : Equivalent circuit model of Schottky-contacted CPW showing contributions of circuit parameters, where Y_{tot} is the total shunt admittance per unit length for the transmission line.

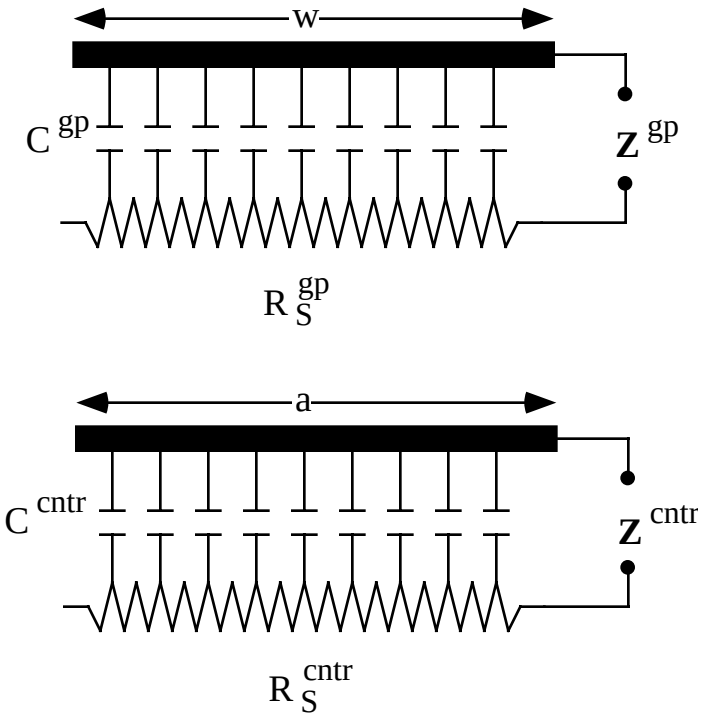

Figure 4.9 : Impedances looking into the center conductor and ground plane when an open circuited R-C transmission line is considered under the CPW conductors.

There is a second order effect of thermionic leakage current which is in parallel to Z^{gp} and Z^{cntr}. To calculate these ac resistances, an ideal diode equation is considered, although the experimental leakage current is an order of magnitude higher than the theoretical value. When these leakage resistances are considered, the new Z^{gp} and Z^{cntr} then become the parallel combination of the old Z^{gp} and Z^{cntr} with corresponding leakage resistances. However, it is observed that these leakage resistances have a very minor effect on the propagation characteristics.

All these effects, when considered to calculate effective shunt admittance, provide good agreement with the experimental results over a wide range of frequencies and bias voltages. The comparisons with low frequency C - V

measurements and with high frequency S-parameter measurements are given in section 4.6.2 and section 4.7, respectively.

4.6 : Low frequency results

Low frequency measurements are primarily performed to ensure "good" Schottky contacts between the CPW electrodes and semiconducting substrate. DC current - voltage measurements provide information regarding the leakage characteristics of the devices. In addition, I-V measurements give actual dc resistances of the CPW electrodes and also of the contacts. Besides I - V, low frequency C - V measurements give the change in capacitance both with bias and with frequency, which is of critical importance in verifying series R effect in the model discussed above. The series R effect and its role in proper interpretation of capacitance-voltage measurements on doped epitaxial layers has been discussed elsewhere [Wiley et al. 1975].

4.6.1 : Current - Voltage characteristics

The Current - Voltage relationship between the signal line and ground plane is simply that of two back-to-back diodes in series. At both polarities, only the leakage current of a reverse-biased diode contributes to the total current. For one polarity, when the center conductor is reverse biased, the leakage current is less than that of ground planes when reverse biased, because of its smaller area. The lower the leakage current density, the better is the Schottky contact between the electrodes and epi layer.

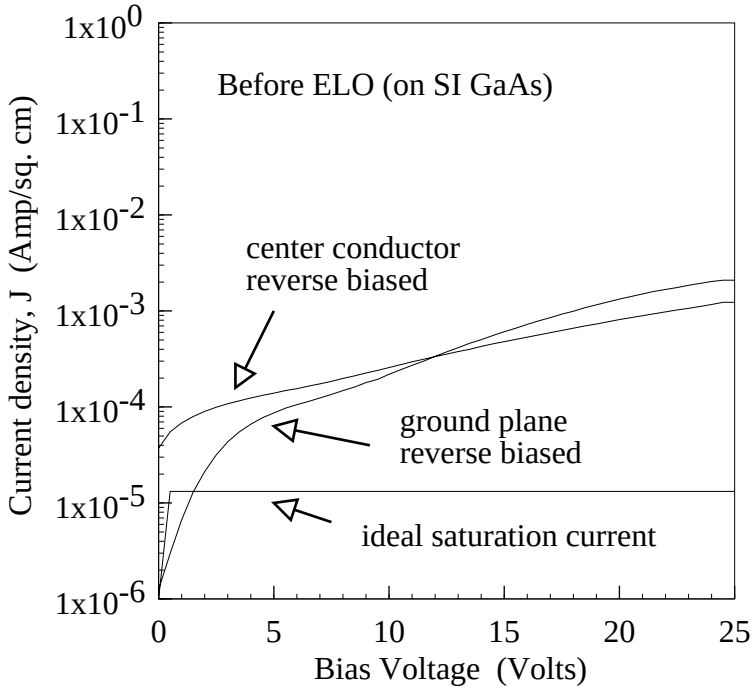

Figure 4.10(a) : Reverse bias current density both for center conductor and ground plane contacts with the epi GaAs layer on top of SI GaAs.

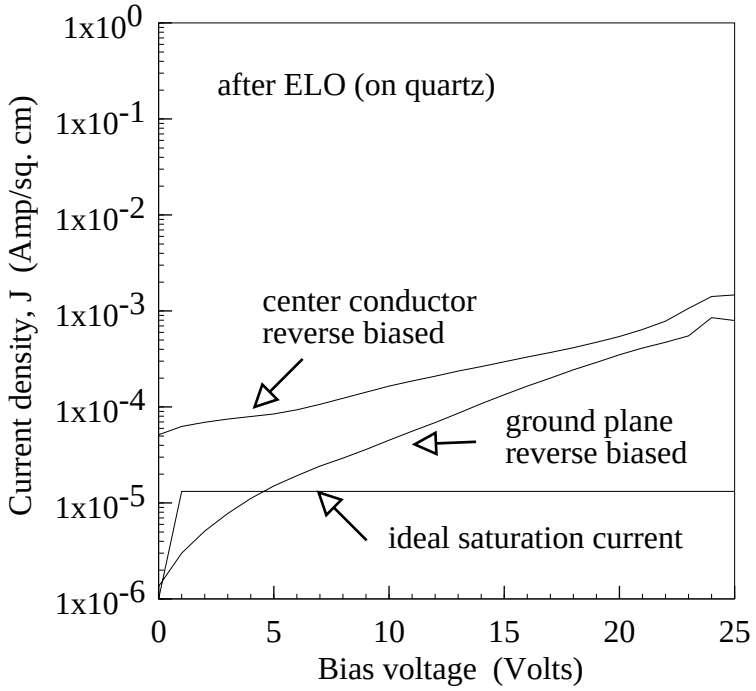

Figure 4.10(b) : Reverse bias current density both for center conductor and ground plane contacts with the epi GaAs layer on top of a Quartz substrate (after epitaxial lift-off).

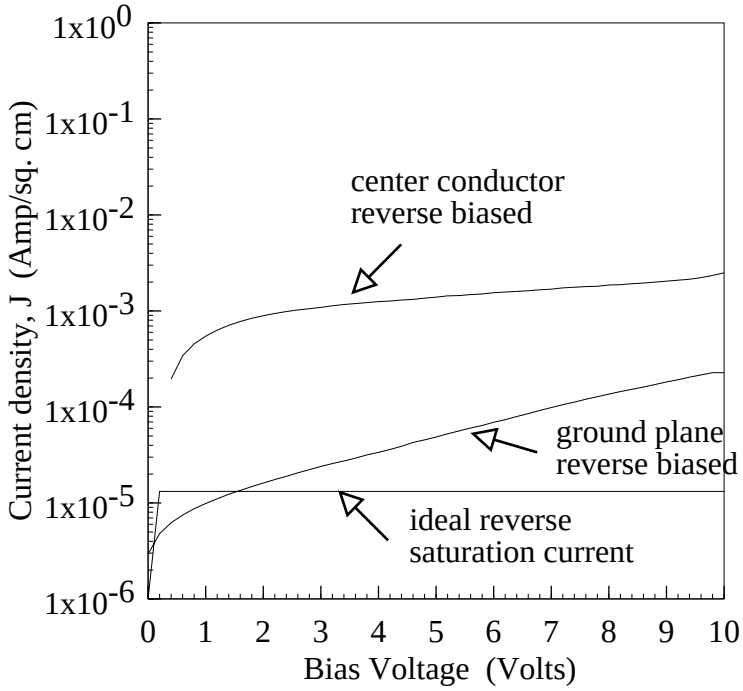

Figure 4.10(c) : Reverse bias current density both for center conductor and ground plane contacts with the 1.5 μm epi GaAs layer on the top SI GaAs substrate.

Measurements of the I - V curves were done with an HP 4140B instrument, which has an input impedance in the range of 10^9 - 10^{10} ohms. Some typical current density (J) versus voltage (V) measurements are shown in Fig. 4.10(a)(b)(c), where a comparison is also made between ideal reverse saturation current [Sze 1981] and the experimental results. Figure 4.10(a) shows the J -V of a 3 μm epi sample on 1000 Å of AlAs on a SI GaAs (before the ELO), whereas the Fig. 4.10(b) shows the J -V characteristics of the epi sample after ELO on a quartz substrate. Comparison between these two figures shows that there is no appreciable degradation in J - V characteristics before ELO and after ELO. Figure 4.10(c) shows the J - V measurements with a 1.5 μm epi layer on top of a thin AlAs

layer on an SI GaAs substrate. In this case, because of the thinner epi layer, the applied voltage is also lower. These plots show that the leakage current is typically an order of magnitude higher than that of an ideal case. However, in calculating the ideal reverse saturation current density only the thermionic leakage current is considered, and one would expect a higher current density at higher reverse voltages, due to tunneling near punch-through. Also it is observed that center conductor always has a higher leakage current density than that of ground planes, and as a result, deviates more from the ideal picture. Usually the breakdown occurs at somewhat lower voltages than the ideal breakdown voltage, but for most cases these breakdown voltages remain higher than the desired operating voltages.

4.6.2 : Capacitance - Voltage characteristics

Small signal capacitance-voltage (C -V) characteristics are important in understanding the device performance from a low frequency perspective. As explained in section 4.6.1, the CPW with the proper bias configuration forms two back to back Schottky diodes with unequal areas. The change in capacitance and in conductance both with voltage and frequency in the low frequency regime (100 kHz - 10 MHz) can be explained from the R_{epi}-C model described in section 4.5. It has been shown that the C - V predicted from the model is in good agreement with that of experimental result.

When the center conductor is biased negative with respect to ground planes for an n-type semi-conductor, the center electrode becomes reverse biased and the ground planes are slightly forward-biased. As both contacts are in series with each other, the reverse biased contact produces most of the voltage drop. The other contact, which is slightly forward biased, drops a very small fraction of the applied bias, typically less than the built-in (due to fermi level pinning of GaAs [Freeouf et al. 1981]) voltage. Therefore, the depletion region under the forward biased junction does not collapse completely, rather the depletion region shrinks a small fraction of the original depleted layer. Due to fermi-level pinning in GaAs a built-in depletion region in the epi-layer is normally present [Look 1989]. As a result,

even without any voltage applied, built-in depletion regions form both from the top and bottom side of the epi layer.

When the center conductor is reverse biased, increasing applied voltage causes the depletion region underneath the center conductor to grow, while the depletion regions under the ground planes remain essentially unchanged. Therefore, the capacitance due to the ground planes ($C_{dep} = \varepsilon_O \varepsilon_r lw / t$) remains constant, where l is the length of the line, but this capacitance is much higher than that under the reverse-biased center conductor, because of larger width (w) and smaller thickness (t). As a result, the overall capacitance is almost completely dominated by the capacitance under the center conductor since they are connected in series. Therefore, until the depletion region under the center conductor reaches the semi-insulating (SI) GaAs substrate, the change of capacitance with voltage behaves the same as that of a normal reversed biased p^+-n junction. In the model calculations, simple depletion approximations are used to evaluate this one-dimensional effect. When full depletion occurs, (i.e., the depletion region under the center conductor reaches the background substrate), the thickness of the depleted layer becomes very large due to the low carrier concentration in the background SI substrate. As a result, the capacitance under the center conductor becomes very small and the quasi-static CPW capacitance, which is in parallel with the depleted region capacitances, dominates. The CPW capacitance is also larger than the forward biased ground planes' capacitances. Therefore, after the full-depletion voltage, where the depletion region reaches the bottom of the epi layer, the overall capacitance remains flat and becomes equal to that of quasi-static CPW capacitance.

When the ground planes are reverse biased with respect to the center conductor, a completely different picture is observed. At lower voltages before full depletion, the capacitance due to depletion region under the ground plane is still higher than that of the center conductor because of its larger width. As a result, the center conductor capacitance, which is caused by the small forward bias voltage, dominates over the ground plane capacitance. Hence the overall capacitance does

not reflect the change in reverse-biased capacitance of the ground planes due to change in voltage, and therefore remains flat at the value set by the forward-biased center conductor capacitance. But when the depletion region reaches the background substrate, the overall capacitance drops by a significant amount due to a series resistance effect [Wiley et al. 1975]. After the full depletion voltage the capacitance remains flat for any higher voltages at a value which is dependent on the background sheet resistance and the frequency of operation. The lower the background sheet resistance or lower the frequency the higher is this flat capacitance value. Higher sheet resistance or higher operating frequency causes the final capacitance to be equal to the quasi-static CPW capacitance. This sharp fall of capacitance due to change in series resistances is the most interesting region, where the CPW is used as an optically-controlled device, since at or near this voltage, even a small perturbation caused by the absorbed photons gives rise to a change in background sheet resistance by a large amount and hence makes the effective capacitance change. In the rf measurements, the optical power is applied at this transition voltage to get the maximum change in propagation constant.

All the C - V measurements were made with an HP4194B Gain-Phase / Impedance Analyzer in conjunction with a Z- probe and tungsten probes at the device end. Prior to any measurement, the calibration of the system was performed over the entire frequency range, which consists of two levels of compensation. The first one calibrates for short (0 ohm), open (0 Siemens) and load (50 ohms) at the Z-probe end, while an offset compensation takes care of short and open calibrations at the tungsten probe end. After each calibration, verification was done with planar chip capacitors and chip resistors. The Gain-Phase Analyzer actually reads the overall impedance data, both real and imaginary parts, and then converts the data into the lumped circuit parameters according to a user specified equivalent circuit. For C - V and C - f measurements, the equivalent circuit chosen was a lumped capacitance in parallel with a lumped conductance.

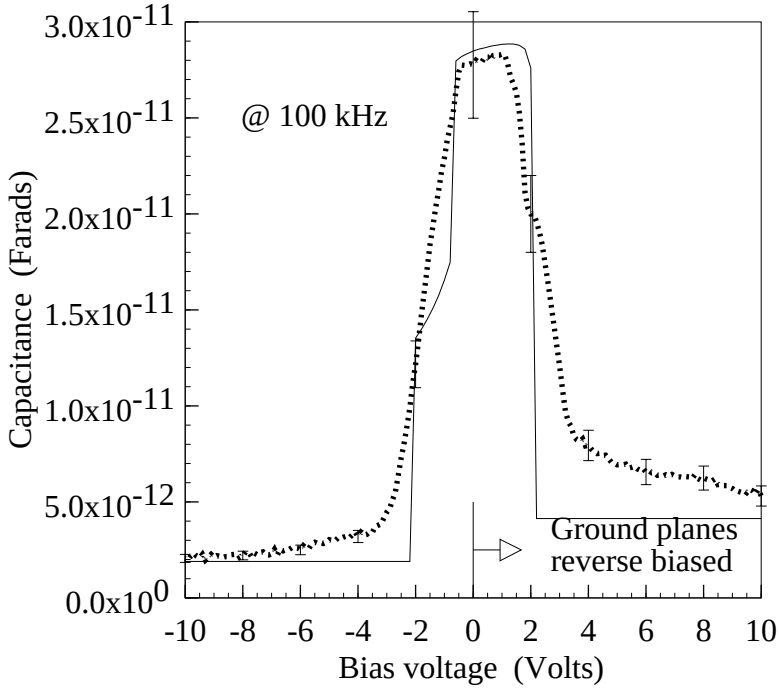

Figure 4.11(a) : Modeled and measured capacitance at 100 kHz. Negative voltage indicates center conductor reverse biased, while positive voltage indicates the ground planes are reverse biased. Bold dotted lines represent experimental result and error bar corresponds to 10% discrepancies in measurements.

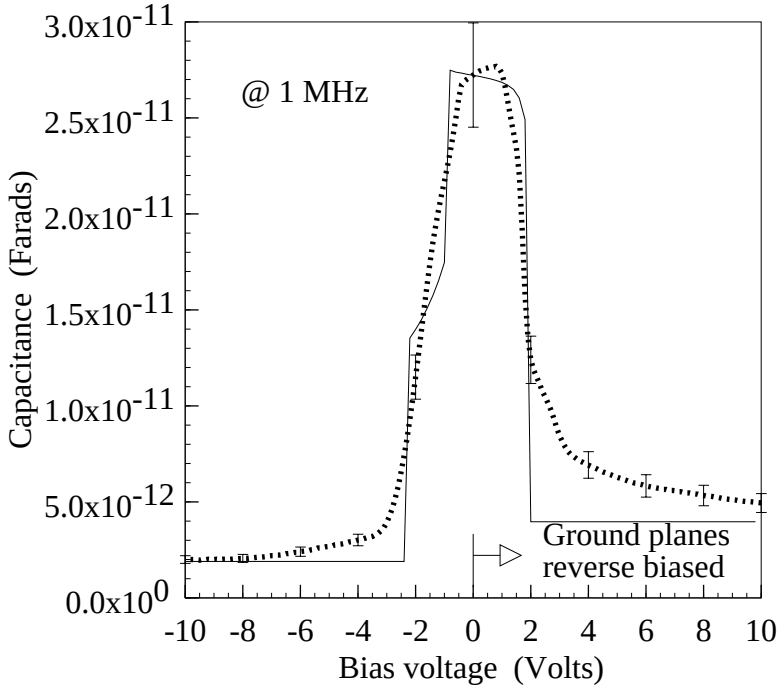

Figure 4.11(b) : Modeled and measured capacitance at 1 MHz. Negative voltage indicates center conductor reverse biased, while positive voltage indicates the ground planes are reverse biased. Bold dotted line represents experimental results and error bars correspond to 10% discrepancies in measurements.

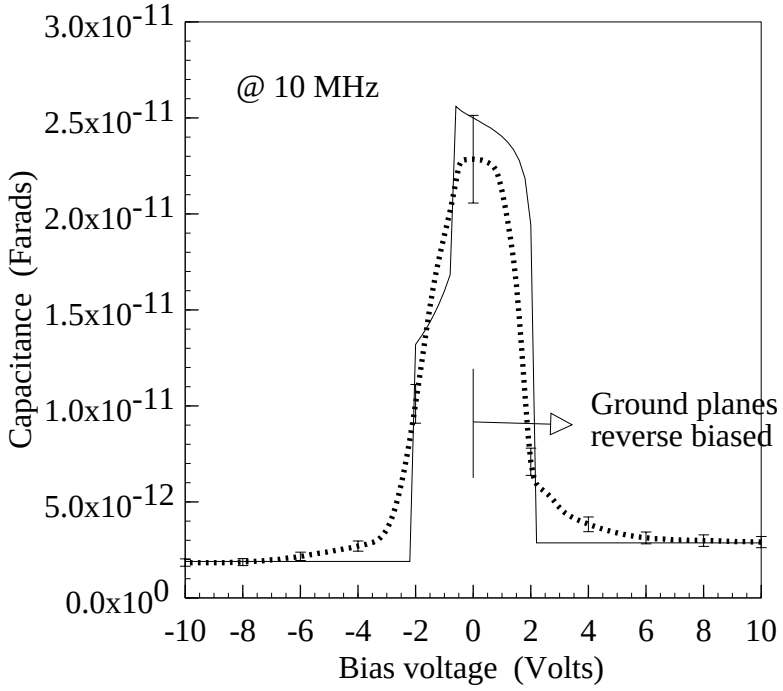

Figure 4.11(c) : Modeled and measured capacitance at 10 MHz. Negative voltage indicates center conductor reverse biased, while positive voltage indicates the ground planes are reverse biased. Bold dotted line represents experimental results and error bars correspond to 10% discrepancies in measurements.

The proposed RC model calculation for both polarities of bias voltages at different frequencies compares well to the experimental results. For the model calculations, the concentration, conductivity and thickness of the epi-layer, and conductivity and thickness of the CPW electrodes were all kept same as that of growth or process conditions. Background sheet resistance is assumed at a constant value of 10^7 ohms, which is fairly consistent with SI GaAs substrate parameters. Measurements were performed by shorting both the ground planes and applying the voltage between the signal line and the ground planes. Error in the measurements were found to be approximately ± 10%. The comparison is made for a sample of

1.5 μm epi GaAs (n-type doping density of approximately $5x10^{15}$ /cm^3) on top of 1000Å AlAs , 2000Å undoped GaAs, and SI GaAs. The metal (silver) thickness is considered to be 1 μm, which is consistent both with deposition conditions and Alpha-step measurement. Comparisons between the model results, using the equation (4.5.12), and measurements are shown in Fig. 4.11(a)(b)(c) at three different frequencies of 100 kHz, 1 MHz and 10 MHz. Error bars are shown for the discrepancies in the measurements. Using the depletion approximations to evaluate one-dimensional depletion thickness in the model gives rise to an abrupt transition from nearly full depletion to complete depletion. In the experimental measurements, this transition is slightly smoother, which is not unexpected if a more realistic drift-diffusion model is considered along with depletion approximations. Furthermore, immediately after the full depletion voltage, the model predicts absolutely no change in capacitance, while experimental data shows a slow drop. Despite these minor discrepancies, the model predicted capacitances against both frequency and voltage are in fairly good agreement with the experimental results.

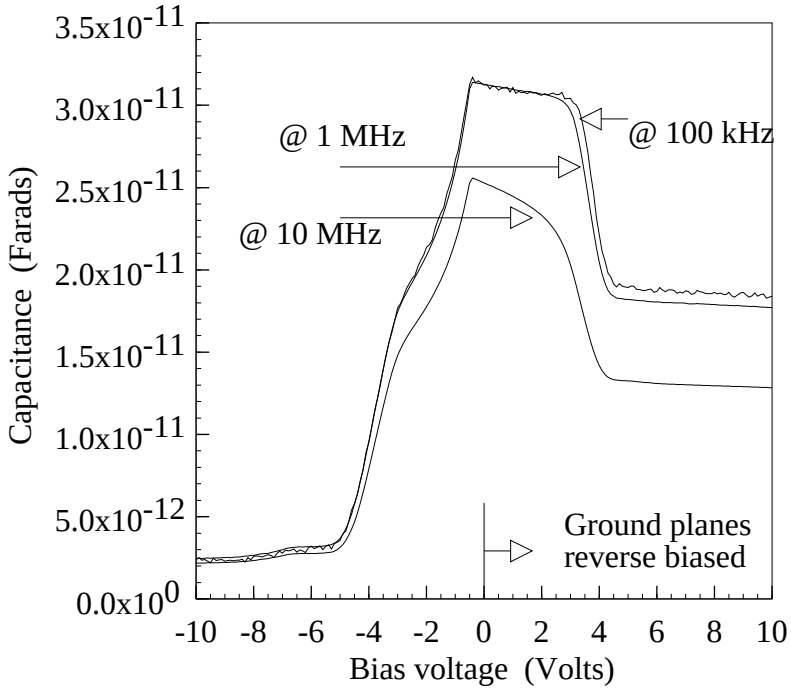

Figure 4.12 : Capacitance voltage measurement at 100 kHz, 1 MHz and 10 MHz.

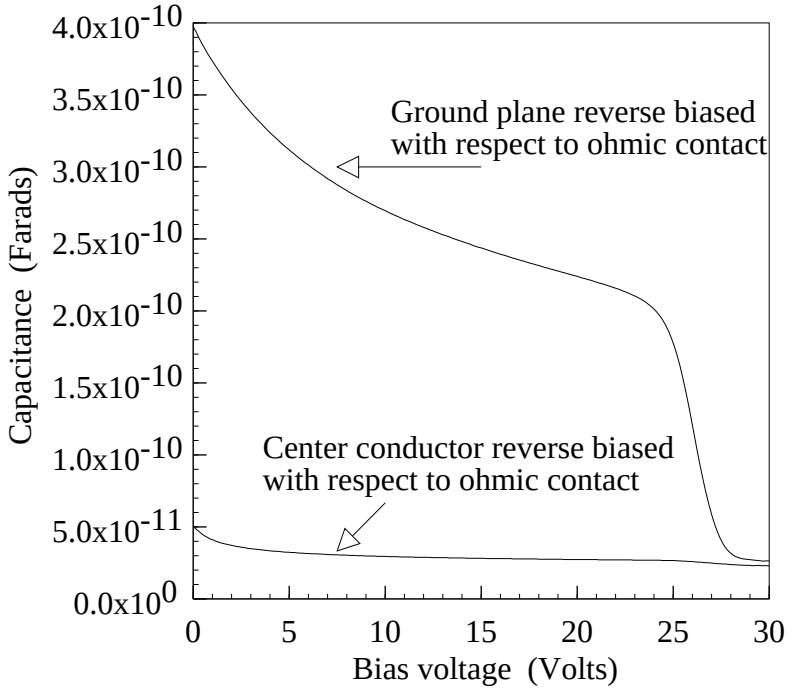

Figure 4.13 : Capacitance voltage measurement at 1 MHz for both center conductor and ground planes reverse biased separately with respect to an ohmic contact.

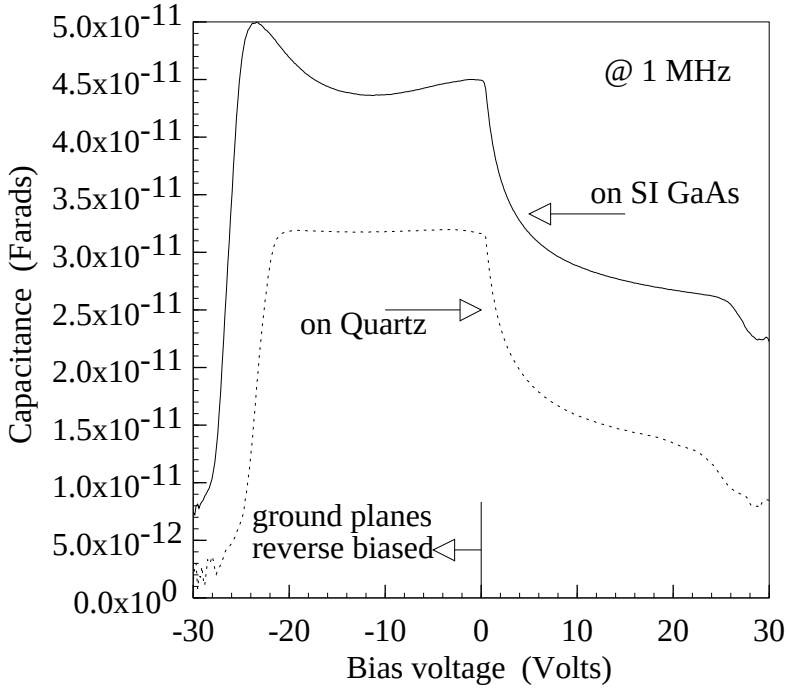

Figure 4.14 : Measured capacitance at 1 MHz before and after ELO.

To further characterize the Schottky-contacted CPW from low-frequency capacitance - voltage measurements, a number of different C -V measurements have also been made. The first plot, Fig. 4.12, shows the variation of measured capacitance against bias voltage between the center conductor and one ground plane at three different frequencies. The sample has a 1.5 μm epi GaAs layer with n-type doping concentration of ~$5x10^{15}$ /cm^3, directly on top of an SI GaAs substrate. It is observed from the plot that lower operating frequency causes the ground plane full-depletion capacitance value to go higher, as well as the zero-bias value. The next plot (Fig. 4.13) shows the variation of capacitance between the center conductor and a separate ohmic contact on the same sample. In the same plot, similar variation is presented for ground plane reverse-biased with respect to

the ohmic contact. From the plot, no flat region at low voltages (when ground planes are reverse biased) is observed. In addition, when the ground plane is reversed biased, the full depletion flat capacitance value is no longer higher than quasi-static CPW capacitance, which further validates the RC model. Another measurement of interest is shown in Fig. 4.14, where a C - V comparison is made between "before" and "after" ELO devices. The "before" ELO CPW consists of a 3 μm epi GaAs on the top of 1000Å AlAs and an SI GaAs substrate, while "after" ELO sample has the same epi layer on the top of a quartz substrate. The epi layer is n-type with $5x10^{15}$ /cm^3 doping concentration. The measurements were performed at an operating frequency of 1 MHz. A distinct difference between the measurements before and after ELO can be observed, mainly because of the higher sheet resistance and much lower dielectric constant of the quartz substrate. The effect of low intensity of optical power on C - V characteristics is shown in Fig. 4.15. Measurements were performed on a 1.5 μm GaAs epi layer with similar doping on the top of thin AlAs and SI GaAs substrate at an operating frequency of 1 MHz. The source of optical power was a broadband microscope illuminator. Even at very low optical power, a significant change in C - V measurements is observed, especially near the sharp transition values.

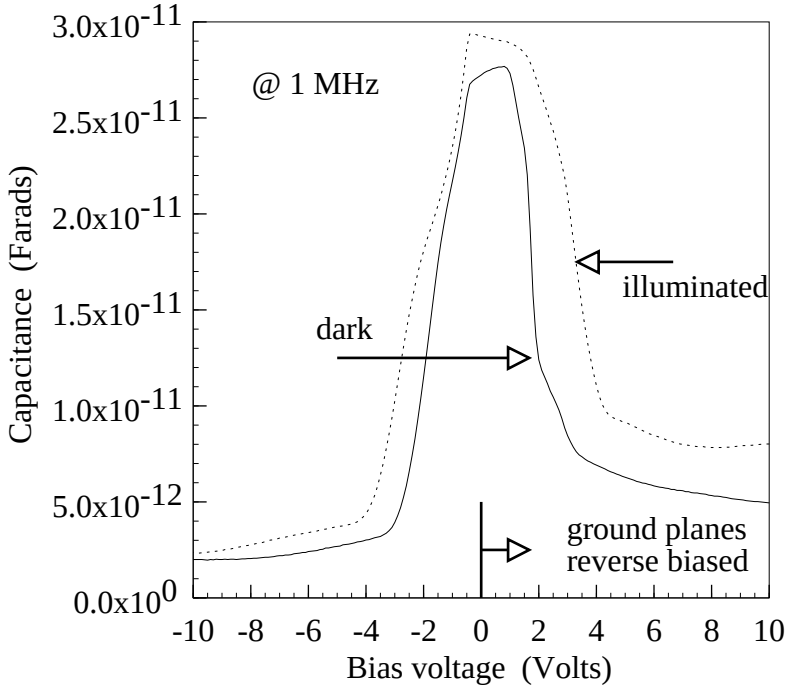

Figure 4.15 : Capacitance voltage measurement for light on and light off conditions.

4.7 : High frequency results

The proposed RC shunt model can also be used to predict the high frequency behavior of the device. From a high frequency perspective, the series resistance effect is more severe than at low frequency. The propagation characteristics reflect the change in capacitance and the corresponding series resistance with the change of bias voltage. Also, at the full-depletion voltage a large change in sheet resistance causes the insertion loss magnitude and phase angle to change by a large amount. At or near that voltage a small perturbation in carrier concentration caused by optical illumination also appears in the propagation characteristics. Besides the shunt model described above, an accurate series impedance per unit length model is also essential for high frequency behavior, since as frequency goes higher both current crowding and skin-effect losses are

larger. For the series model, a quasi-static conformally mapped model as discussed in chapter 3, is used. To include the effect of the lossy epi layer on the total inductance of the device an additional resistance and inductance in parallel with previous R_{series} and L_{series} (based on conformal mapping), is included in the overall series circuit. To model this lossy layer inductive term, a quasi-static parallel plate inductance between the center conductor and the conducting layer underneath it, is assumed. A more appropriate model would be a microstrip like inductance between the center conductor and the lossy layer. In the simple case, as shown in Fig. 4.16, these resistances and inductances are modeled as

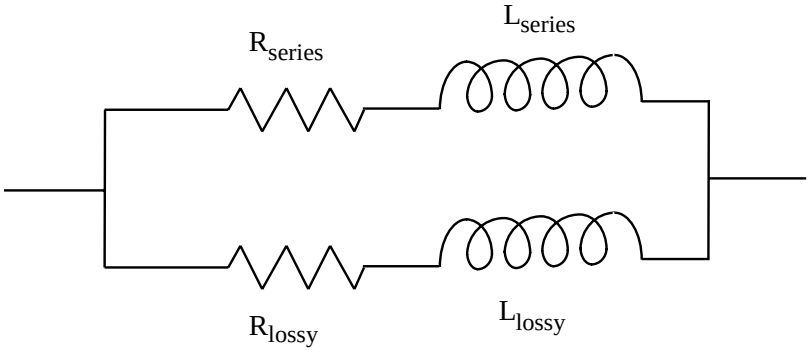

Figure 4.16 : Equivalent series impedance model to consider the effect of the lossy semi-conducting layer on the CPW metal lines.

$$L_{lossy} = \frac{\mu_o h}{2a} \tag{4.7.1}$$

$$R_{lossy} = \frac{R_s}{2a} \tag{4.7.2}$$

where $R_S = 1/t\sigma$, t and σ being the thickness and conductivity of the lossy layer respectively, and h being the thickness of the top depleted layer. a is half of the

center conductor width. R_{lossy} measures the series resistance of a wire *2a* wide that is *t* thick with conductivity σ. The contribution from this lossy arm in the series circuit has very little effect on propagation characteristics at all voltages, but it is still considered in the model because it carries a measure of the resistance in the conducting layer on the Z-ckt. The rest of the model parameters are the same as those used for low frequency comparisons.

All experimental measurements were done with an HP 8510B Automatic Network Analyzer in conjunction with ground-signal-ground (GSG) wafer probes. With the Network Analyzer, S-parameters were measured at different bias conditions over the full frequency range of 45 MHz to 40 GHz. Prior to any measurements, a full 2-port calibration was performed at the probe end, which included open, short, and load (50 ohms) for each probe and through compensation between two probes. Attenuation constant, α (db/cm), effective index of refraction (n_{eff}), and characteristic impedance (Z_o) were all derived from the measured S-parameters. Comparisons are made between the experiment and model for attenuation constant, n_{eff}, and effective capacitance (derived from imaginary part of propagation constant) at different bias conditions. Comparisons are made for the same sample that has been used for low frequency C-V comparison. Different bias conditions include one at zero bias, and two each for ground planes reverse biased (at 2V and 7V) and center conductor reverse biased (at 2V and 7V). From the rf measurements, it was observed that the propagation constant slowly changes even after the full depletion voltage, predicted from a simple one-dimensional depletion approximation, and ceases to change at somewhat higher voltage. The RC model fails to predict this feature since the simple depletion approximation cannot capture the full one-dimensional effects completely. However, the model can predict the results correctly for any voltage before the full depletion and also at some higher voltage after which no changes are detected. "No change" voltage is where both the epi layer and SI substrate are fully depleted, which the model predicts at immediately after the "full depletion" voltage. The comparisons are shown in Fig. 4.17, Fig. 4.18 and in Fig. 4.19. In Fig. 4.17(a) and (b), attenuation constant and

effective index of refraction at positive voltages applied to the center conductor are shown for comparison. Positive voltage applied to the center conductor means ground planes reverse biased with center conductor slightly forward biased. Figure 4.18(a) and (b) show the similar comparison at negative bias applied to the center conductor, which means center conductor reverse biased with respect to two ground planes. In Fig. 4.19(a) and (b), comparisons are shown for effective capacitances in the shunt circuit at positive and negative voltages applied to the signal line, respectively. Other parameters, including effective conductance or real and imaginary parts of characteristic impedance also show a good match between the measured and simulated results. All these comparisons demonstrate the validity of this simple model, and also explain the main parameters that determine the propagation constant of a Schottky-contacted CPW on a lightly-doped GaAs layer on an SI substrate.

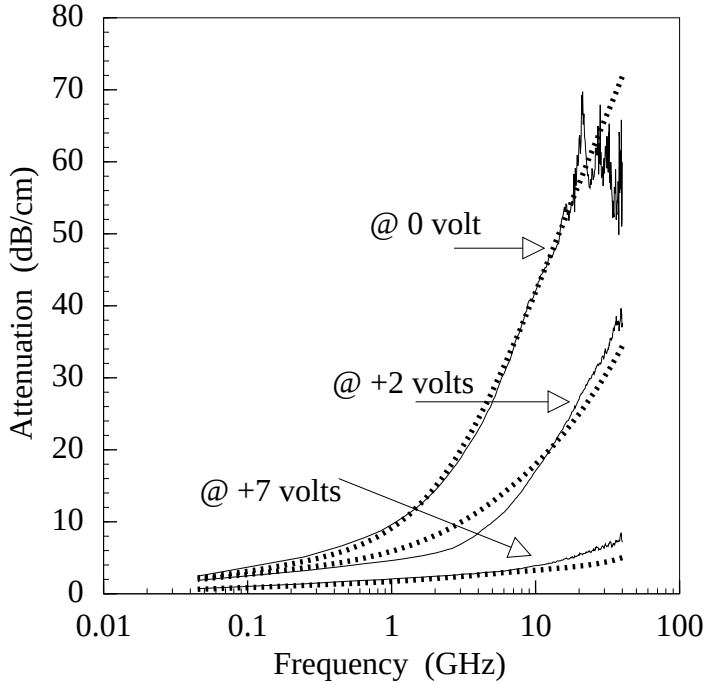

Figure 4.17(a) : Measured and modeled results for attenuation constant at three biasing conditions (ground planes reverse biased, and 7 V being the full depletion voltage). Dotted lines represent simulated results.

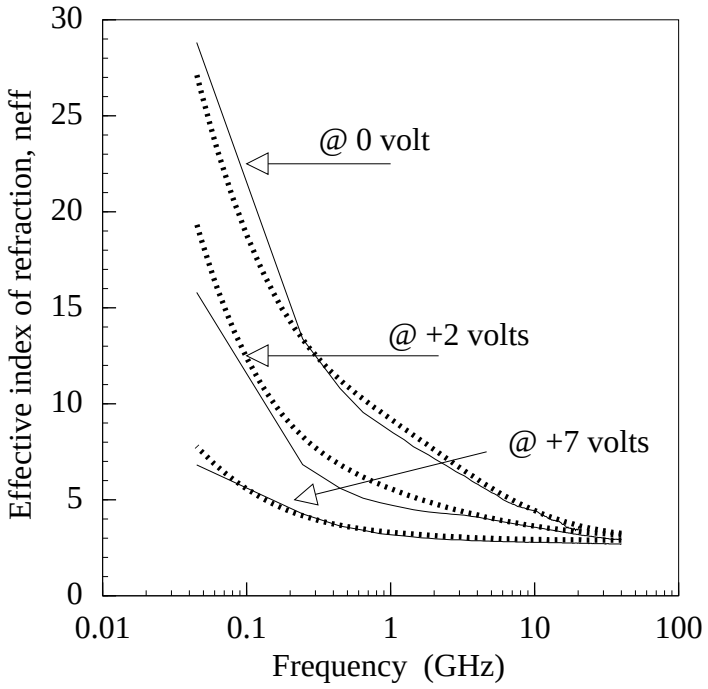

Figure 4.17(b) : Measured and modeled results for effective index of refraction (n_{eff}) at three biasing conditions (ground reverse biased, and 7 V being the full depletion voltage). Dotted lines represent simulated results.

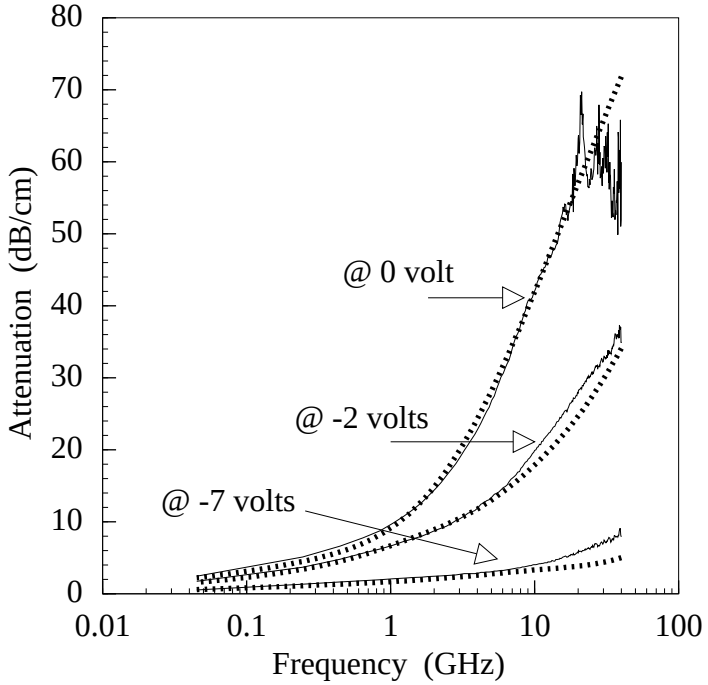

Figure 4.18(a) : Measured and modeled results for attenuation constant at three biasing conditions (center conductor reverse biased, and -7 V being the full depletion voltage). Dotted lines represent simulated results.

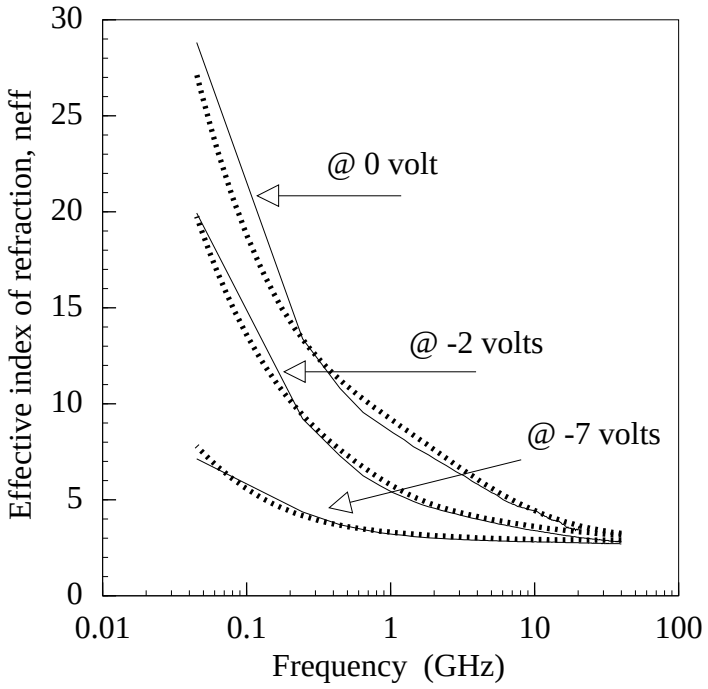

Figure 4.18(b) : Measured and modeled results for effective index of refraction (n_{eff}) at three biasing conditions (center reverse biased, and -7 V being the full depletion voltage). Dotted lines represent simulated results.

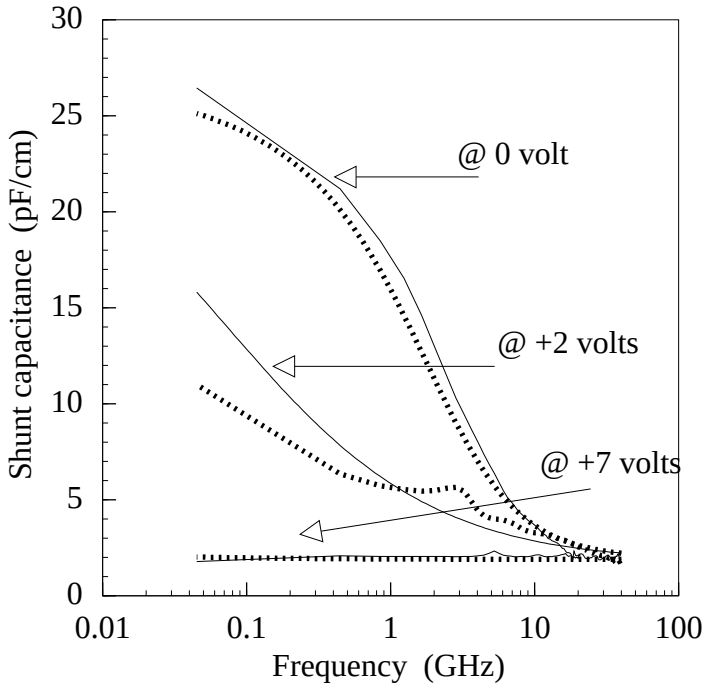

Figure 4.19(a) : Measured and modeled results for effective shunt capacitance at three biasing conditions (ground reverse biased, and 7 V being the full depletion voltage). Dotted lines represent simulated results.

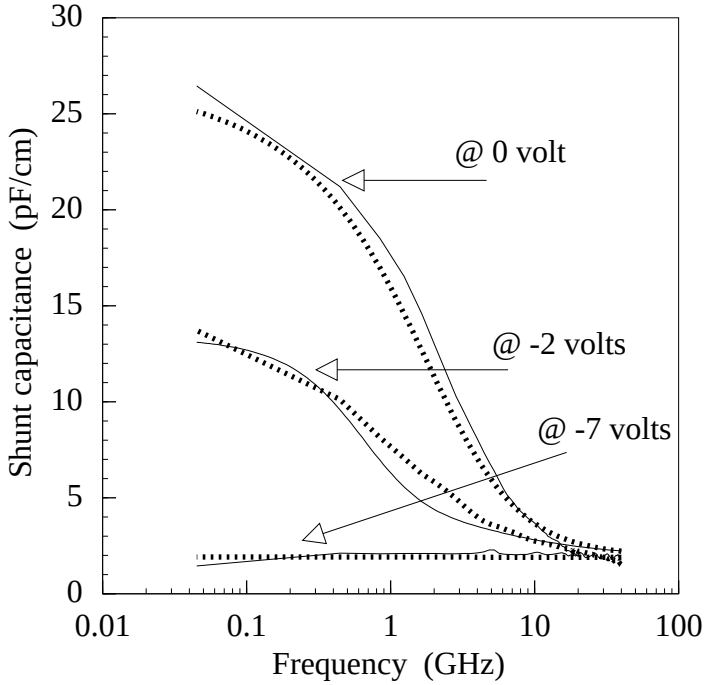

Figure 4.19(b) : Measured and modeled results for effective shunt capacitance at three biasing conditions (center reverse biased, and -7V being the full depletion voltage). Dotted lines represent simulated results.

4.8 : Model results for MIS (Metal-Insulator-Semiconductor) structures

The proposed R_{epi}-C model is able to predict results for a true MIS (Metal-Insulator-Semiconductor) structure as well, which supports a slow-wave mode of propagation along the transmission line. Usually an MIS structure consists of metal electrodes, a true insulator (such as SiO_2 or $Al_xGa_{1-x}As$) and a semiconducting layer (such as Si or GaAs). Other investigators [Guckel et al. 1967; Hasegawa et al. 1971; Jager et al. 1974; Jager 1976; Shih et al. 1982; Fukuoka et al. 1983; Seguinot et al. 1983; Sorrentino et al. 1984; Seguinot et al. 1986; Tzuang et al. 1986; Kwon et al. 1987; McKaughan et al. 1988; Shibata et al. 1990; Liou et al.

1993] analyzed these coplanar structures for slow-wave mode propagation using various methods, which include both full-wave treatment and quasi-TEM analysis. The full-wave analyses are based on mode-matching method [Fukuoka et al. 1983; Sorrentino et al. 1984], spectral-domain analysis method [Shih et al. 1982] [Liou et al. 1993], finite element method [Tzuang et al. 1986], finite difference time domain method (FDTD) [Shibata et al. 1990], etc. Among the quasi-TEM analyses [Jager et al. 1974; Jager 1976; Seguinot et al. 1983; Sorrentino et al. 1984; Seguinot et al. 1986; Kwon et al. 1987; Nary et al. 1993], different equivalent circuit models are presented but most of them with limited success, especially for a wide range of semiconductor resistivity and when conductor losses are included. The R_{epi}-C model proposed in this chapter, along with the conductor loss model discussed in chapter 3, is able to predict the propagation characteristic along a Schottky or a MIS coplanar line with fair accuracy. Champlin's model results [Kwon et al. 1987] and their experimental work are compared with the proposed R_{epi}-C model, which verifies the validity of the model even for an ideal slow-wave structure. Besides Champlin's experimental work, measurements have also been performed on a CPW SiO_2-Si structure (made by E. Tuncer) up to 40 GHz and then compared with both Champlin's model and our proposed model.

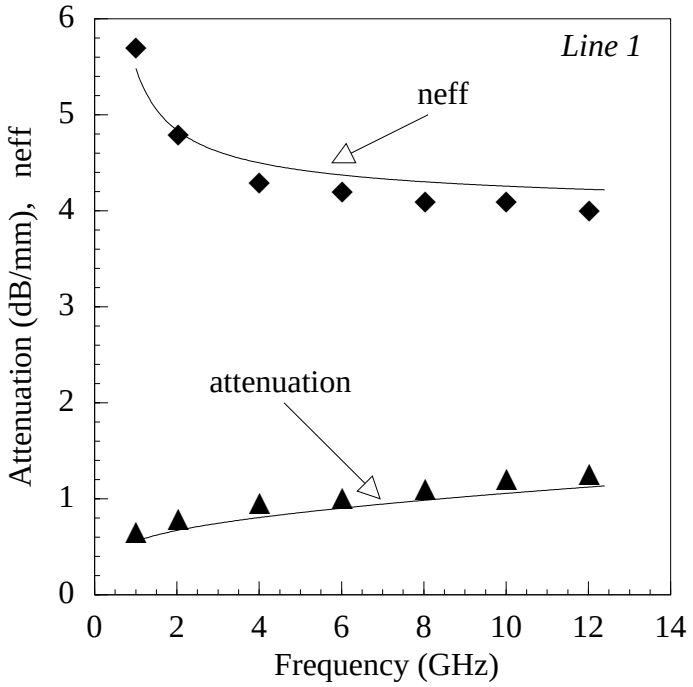

Figure 4.20 : Comparison of attenuation constant and effective refractive index (n_{eff}) between Champlin's experimental results for CPW line 1 structure [Kwon et al. 1987] and our R_{epi}-C model results.

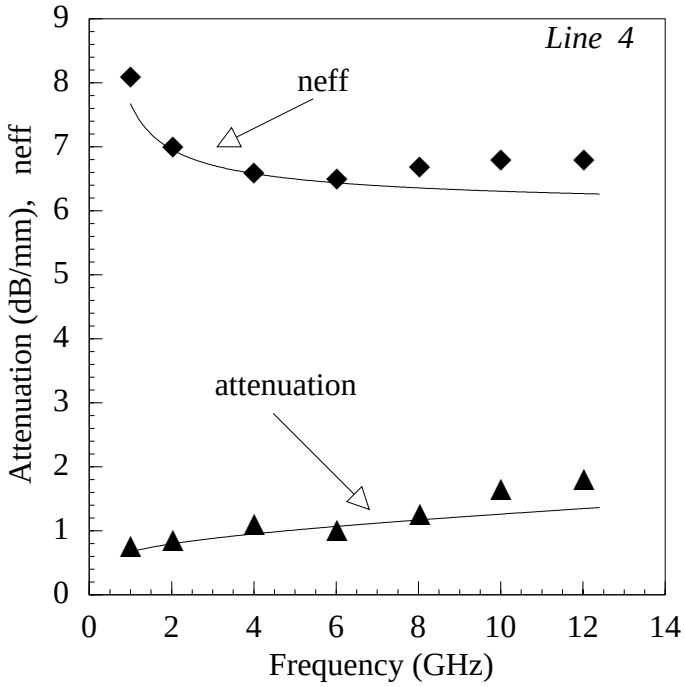

Figure 4.21 : Comparison of attenuation constant and effective refractive index (n_{eff}) between Champlin's experimental results for CPW line 4 structure [Kwon et al. 1987] and our R_{epi}-C model results.

To use the R_{epi}-C model as proposed in this chapter, calculation of effective sheet resistance of the semiconductor layer is very important. When the semiconductor layer is very thick compared to the width of the electrodes, it can be approximated as

$$R_s^{eff} = \frac{\rho}{w} \tag{4.8.1}$$

where ρ and w are the resistivity of the semiconductor layer and the width of the electrode respectively. When these effective sheet resistances are used with the R_{epi}-C model, the results show fairly good agreement with the experimental results. First of all, the modeled results are compared with the experimental work

performed by Champlin et al. [Kwon et al. 1987] , which are shown for two different transmission lines in Fig. 4.20 and Fig. 4.21. In Fig. 4.20, comparisons are shown for attenuation and slow-wave factor (n_{eff}) for line 1 and similar comparisons are shown in Fig. 4.21 for line 4. All these experimental results were performed only up to 12 GHz, and show good agreement both with Champlin's model and our model. A higher frequency (up to 40 GHz) experimental work, done by us, based on a much higher resistivity Si substrate is again compared with Champlin's and our models, shown in Fig. 4.22(a) & (b). In this comparison it is clear that Champlin's model visibly fails to accurately predict the propagation characteristics of the coplanar MIS transmission line at higher frequencies, whereas our model still agrees well with the experimental work even into the millimeter wave regime.

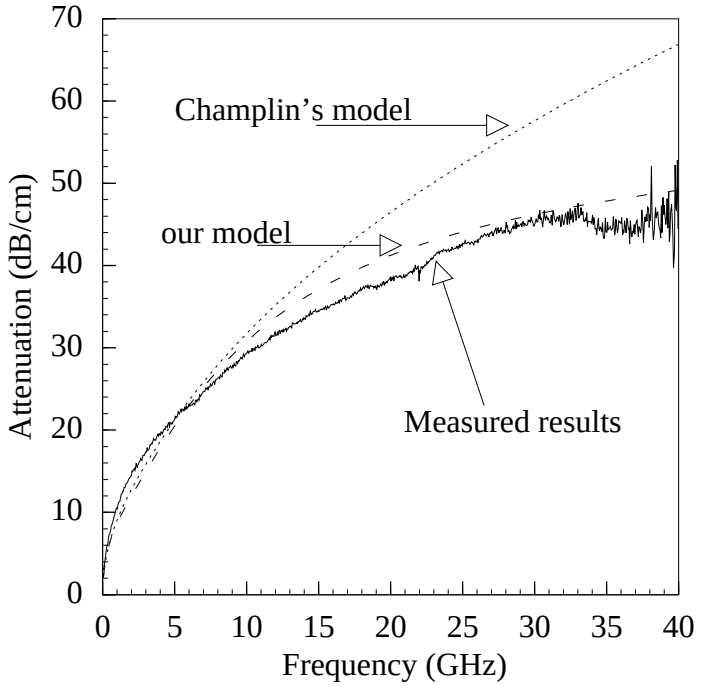

Figure 4.22(a) : Comparison of measured attenuation constant with the R_{epi}-C model and Champlin's model [Kwon et al. 1987] for a Si-SiO_2 CPW structure.

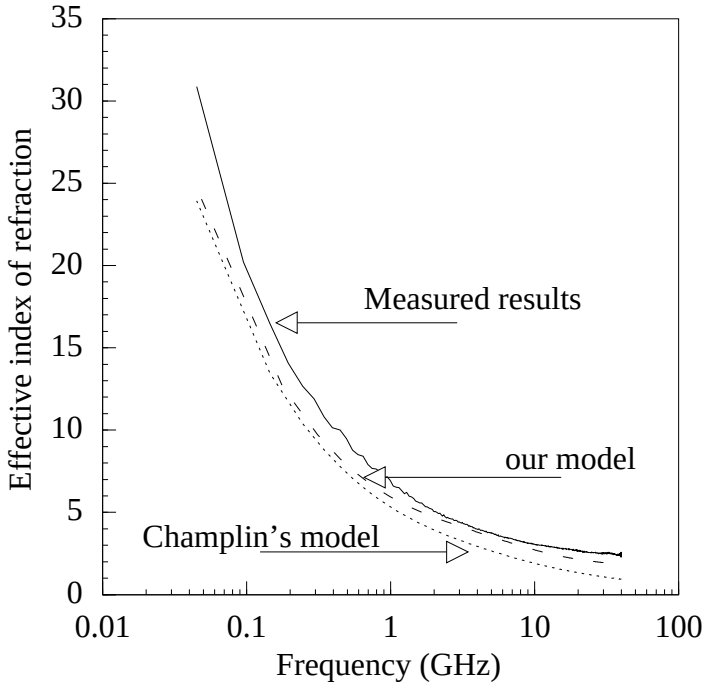

Figure 4.22(b) : Comparison of measured effective refractive index (n_{eff}) with the R_{epi}-C model and Champlin's model [Kwon et al. 1987] for a Si-SiO_2 CPW structure.

4.9 : Effect of backside sheet resistance

As already discussed in previous sections, the proposed R_{epi}-C model can explain the main mechanism of rf propagation in a Schottky-contacted CPW. In this section, the effect of backside sheet resistance on the attenuation and effective index of refraction of a distributed CPW is discussed. As backside sheet resistance is one of the deciding factors in rf propagation along this planar transmission line, it is worth mentioning the dependence of propagation constant of the transmission line on the back sheet resistance. The proposed R_{epi}-C model is used to simulate this dependence, where a fixed insulator thickness is considered with variable backside sheet resistance for a CPW. An interesting feature is obtained in these

simulated results, where attenuation of the line shows a "double hump" characteristic at all rf frequencies. Attenuation peaks at two different sheet resistances, with a minimum value at an intermediate point. The intermediate minimum attenuation value corresponds to a high value of n_{eff}. An optimized sheet resistance can be identified because of this feature, where this sheet resistance value causes lower attenuation and higher n_{eff}. Figure 4.23 and Fig. 4.24 show the variation of both attenuation and n_{eff} with changing sheet resistances, ranging from the value of 10^{-3} ohm per square to 10^{10} ohms per square. Figs. 4.23(a) & (b) show the variation at different frequencies with one fixed insulator thickness (0.5 μm), while figs. 4.24(a) & (b) are calculated for one particular frequency (30 GHz) with different insulator thicknesses. From the Fig. 4.23, it can be observed that at one particular insulator thickness, increasing operating frequency causes optimum R_s (intermediate value where minimum attenuation and maximum n_{eff} occur) to remain the same, but R_s corresponding to first peak moves to right (higher sheet R), whereas second peak shifts to left (lower sheet R value). Also, with increasing frequency, the value of n_{eff} is lowered and the width of flat high n_{eff} region is decreased. The same optimum R_s at different frequencies makes this R_S attractive for practical implementation of low attenuation and high n_{eff} microwave devices. If the insulator thickness is varied at one particular frequency, as evidenced from Fig. 4.24, increasing thickness causes sheet R corresponding to both the first peak, and second peak to shift to the right (to higher values of R_s). Increasing thickness causes n_{eff} to decrease as well, as observed in Fig. 4.24(b).

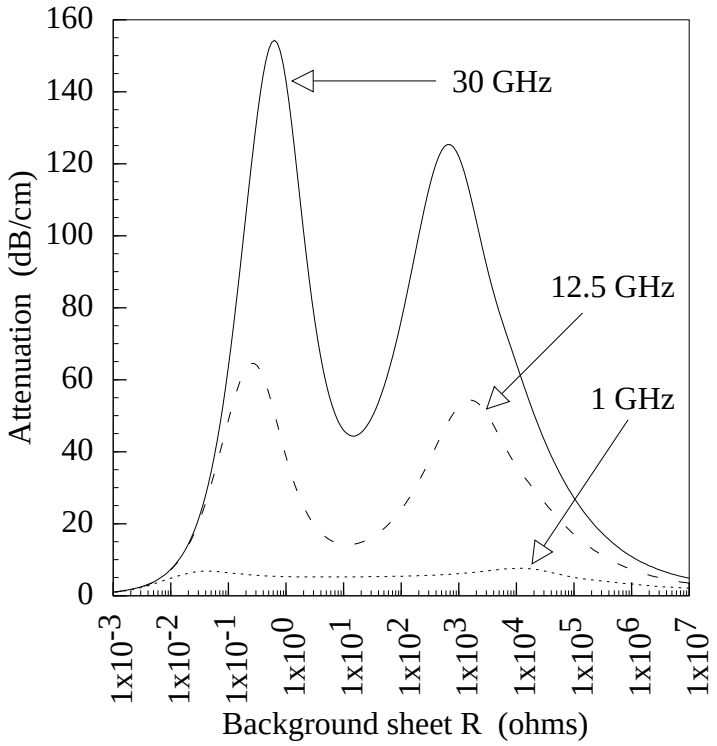

Figure 4.23(a) : Simulated results of attenuation constant (dB/cm) as a function of background sheet resistance at different frequencies with a fixed insulator thicknesses of 0.5 μm.

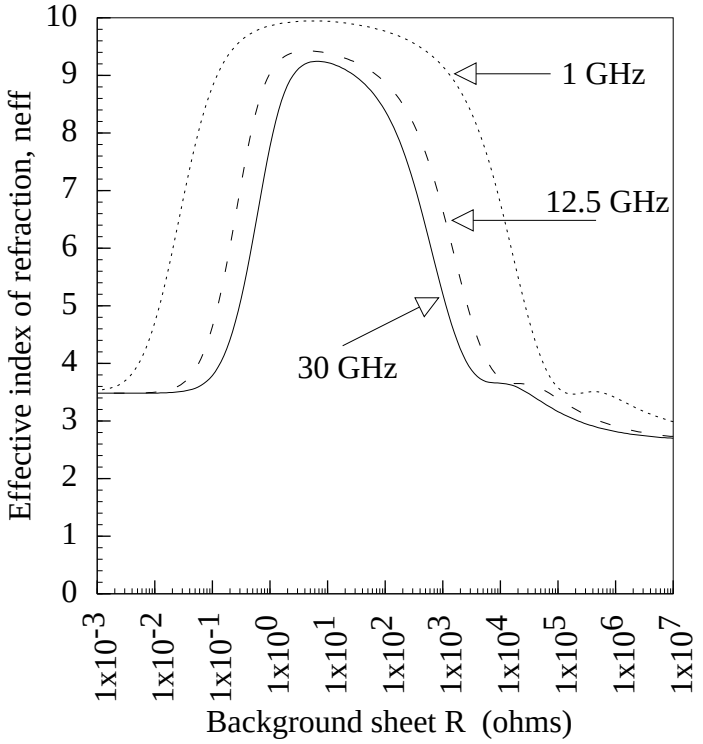

Figure 4.23(b) : Simulated results of effective index of refraction (n_{eff}) as a function of background sheet resistance at different frequencies with a fixed insulator thicknesses of 0.5 μm.

The first peak at lower sheet resistance corresponds to the effect of the back sheet resistance on the series impedance of the line (due to micro-strip like effects as shown in Fig. 4.16), while the second peak corresponds to loss associated with the shunt circuit. At very low R_s, where loss drops down from the first peak, the transmission line works more like a microstrip line, with metal-like behavior of the lossy layer in the substrate. At very high R_s, loss again drops down from the second peak, because now the substrate almost works as an insulator, where loss is minimal. Both with very low and very high R_s values, lower attenuation

correspond to lower effective index of refraction too. Only at intermediate values of R_S between the two peaks are losses low and at the same time n_{eff} high. Experimentally, to obtain this optimum back sheet resistance, the ELO technique was used to transfer a thin epitaxial layer of GaAs onto a 100-200Å Palladium-plated glass slide, with the CPW electrodes on the top of GaAs layer. Several attempts failed because of processing failures during the epitaxial lift off, resulting in devices that were shorted. As a result, thus far it has not been possible to experimentally verify the simulated results of propagation constant of the CPW.

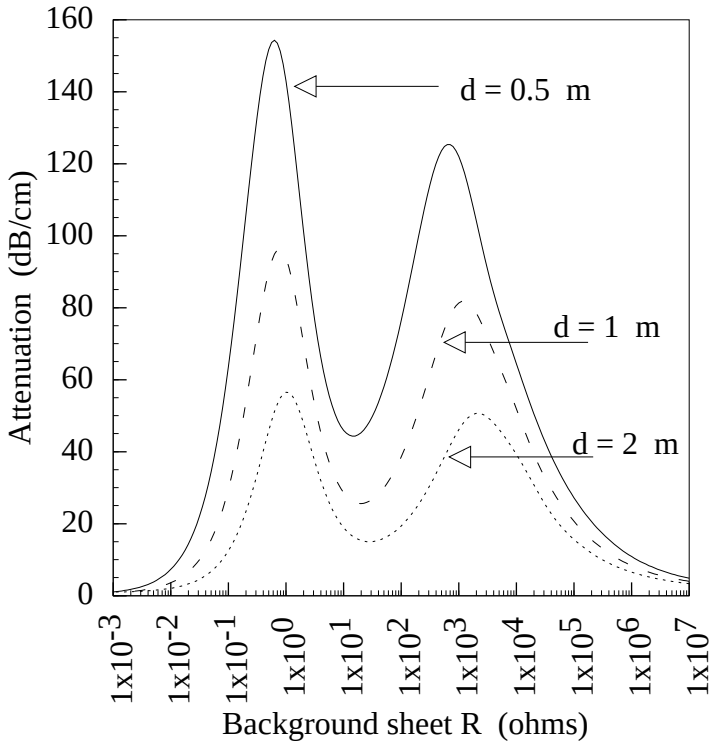

Figure 4.24(a) : Simulated results of attenuation constant (dB/cm) as a function of background sheet resistance with different insulator thicknesses (d) at a fixed frequency of 30 GHz.

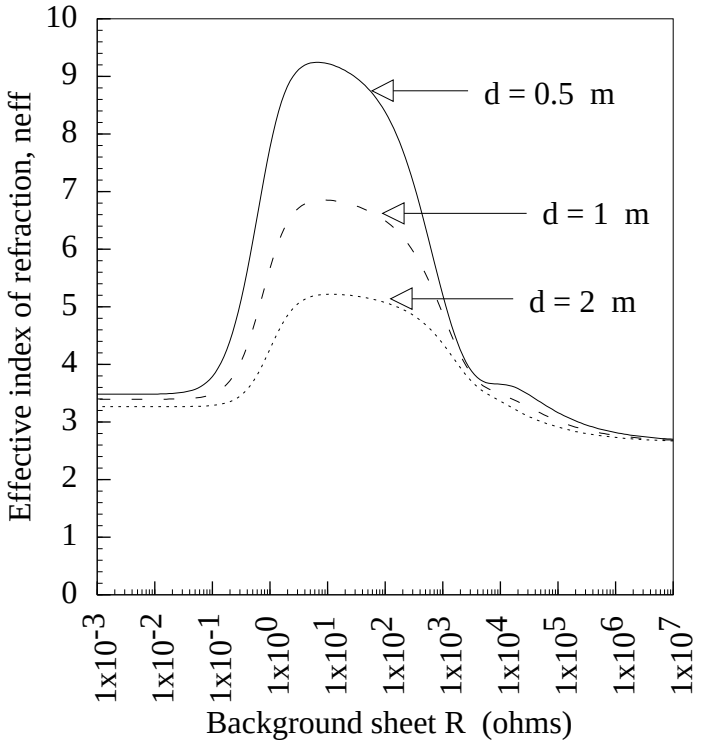

Figure 4.24(b) : Simulated results of effective index of refraction (n_{eff}) as a function of background sheet resistance with different insulator thicknesses (d) at a fixed frequency of 30 GHz.

4.10 : Summary

In this chapter, a new, complete equivalent circuit model has been presented for a Schottky or a MIS coplanar transmission line structure, which provides a better understanding of the main propagation mechanism along the distributed transmission line. To derive the equivalent circuit model, a distributed capacitance with the series resistance in the semiconductor layer is used, which provides good agreement with the experimental results for a wide range of line geometries and semiconductor resistivities. The complete model also incorporates the conductor loss calculation already discussed in chapter 3. To support the proposed R_{epi}-C

model both low (dc - 10 MHz) and high frequency (45 MHz - 40 GHz) characterization has been performed, in terms of capacitance - voltage (C-V), capacitance - frequency (C-f) and S-parameter measurements. The model described in this chapter is simple in conception, analytic in nature, numerically efficient, and at the same time provides good agreement with the experimental results. The model can be useful for analyzing coplanar MIS or Schottky transmission lines, used in high speed digital integrated circuits or in monolithic microwave integrated circuit (MMIC) applications.